AGU PUBLICATIONS

JGR

Journal of Geophysical Research: Earth Surface

RESEARCH ARTICLE
10.1002/2014JF003392

Key Points:
- Meandering rivers undergoing steady incision create autogenic terraces
- Autogenic terraces can be paired and longitudinally extensive
- Autogenic terraces have timescales that can overlap with climate forcing

Supporting Information:
- Captions for Movies S1–S7
- Movie S1
- Movie S2
- Movie S3
- Movie S4
- Movie S5
- Movie S6
- Movie S7

Correspondence to:
A. B. S. Limaye,
aslimaye@umn.edu

Citation:
Limaye, A. B. S., and M. P. Lamb (2016), Numerical model predictions of autogenic fluvial terraces and comparison to climate change expectations, *J. Geophys. Res. Earth Surf.*, *121*, doi:10.1002/2014JF003392.

Received 14 NOV 2014
Accepted 2 FEB 2016
Accepted article online 8 FEB 2016

Numerical model predictions of autogenic fluvial terraces and comparison to climate change expectations

Ajay B. S. Limaye[1,2] and Michael P. Lamb[1]

[1]Division of Geological and Planetary Sciences, California Institute of Technology, Pasadena, California, USA, [2]Now at St. Anthony Falls Laboratory, University of Minnesota, Twin Cities, Minneapolis, Minnesota, USA

Abstract Terraces eroded into sediment (alluvial) and bedrock (strath) preserve an important history of river activity. River terraces are thought to form when a river switches from a period of slow vertical incision and valley widening to fast vertical incision and terrace abandonment. Consequently, terraces are often interpreted to reflect changing external drivers including tectonics, sea level, and climate. In contrast, the intrinsic unsteadiness of lateral migration in rivers may generate terraces even under constant rates of vertical incision without external forcing. To explore this mechanism, we simulate landscape evolution by a vertically incising, meandering river and isolate the age and geometry of autogenic river terraces. Modeled autogenic terraces form for a wide range of lateral and vertical incision rates and are often paired and longitudinally extensive for intermediate ratios of vertical-to-lateral erosion rate. Autogenic terraces have a characteristic reoccurrence time that scales with the time for relief generation. There is a preservation bias against older terraces due to reworking of previously visited parts of the valley. Evolving, spatial differences in bank strength between bedrock and sediment reduce terrace formation frequency and length, favor pairing, and can explain sublinear terrace margins at valley boundaries. Age differences and geometries for modeled autogenic terraces are consistent, in cases, with natural terraces and overlap with metrics commonly attributed to terrace formation due to climate change. We suggest a new phase space of terrace properties that may allow differentiation of autogenic terraces from terraces formed by external drivers.

1. Introduction

River terraces are low-relief surfaces perched above the channel and formed by deposition and erosion of valley-fill sediments (i.e., alluvial terraces) or erosion of bedrock (i.e., strath terraces) [*Bucher*, 1932; *Bull*, 1991; *Pazzaglia*, 2013]. The geometry and number of terraces differ widely. For example, terraces may be contiguous and occupy several topographic levels (e.g., Clearwater River valley, Washington; Figure 1a) or may be separated and less numerous (e.g., Mattole River valley, California; Figure 1b). In some locations terraces are particularly wide and long (e.g., Colorado River valley, Texas, Figure 1d, and Wind River valley, Wyoming, Figure 1e), with boundaries that are closely (Figure 1d) or loosely (Figure 1e) associated with the neighboring river channel. Terraces are globally distributed [*Montgomery*, 2004; *Bridgland and Westaway*, 2008] and span a range of physiographic environments, including coastal mountain ranges (e.g., Figures 1a and 1b), continental interiors (e.g., Figures 1c and 1e), and broad coastal plains (e.g., Figure 1d).

Terraces can preserve a record of channel evolution for hundreds of thousands of years [*Pan et al.*, 2003]. Consequently, river terraces are the principal geomorphic features for reconstructing channel aggradation and incision and one of the key constraints on long-term sediment fluxes from landscapes [*Bull*, 1991; *Fuller et al.*, 2009] to marine depositional basins [*Blum and Aslan*, 2006; *Phillips and Slattery*, 2006]. Tectonic studies also frequently use terraces as passive markers of deformation and rock uplift [*Rockwell et al.*, 1984; *Personius*, 1995; *Pazzaglia et al.*, 1998; *Lavé and Avouac*, 2000].

Terrace formation requires valley widening to bevel terrace treads and vertical incision to abandon these surfaces above the channel [*Hancock and Anderson*, 2002; *Montgomery*, 2004; *Bridgland and Westaway*, 2008]. A change in the ratio of vertical-to-lateral erosion rate is commonly cited as a requirement for terrace formation [*Hancock and Anderson*, 2002; *Fuller et al.*, 2009; *Finnegan and Dietrich*, 2011; *Langston et al.*, 2015] and is usually attributed to changes in vertical incision rate driven by external factors, including tectonics [*Bull*, 1991; *Demir et al.*, 2009; *Yanites et al.*, 2010; *DiBiase et al.*, 2014], base level change [*Fisk*, 1944; *Pazzaglia and Gardner*, 1993; *Blum and Tornqvist*, 2000; *Finnegan and Balco*, 2013], and, most frequently,

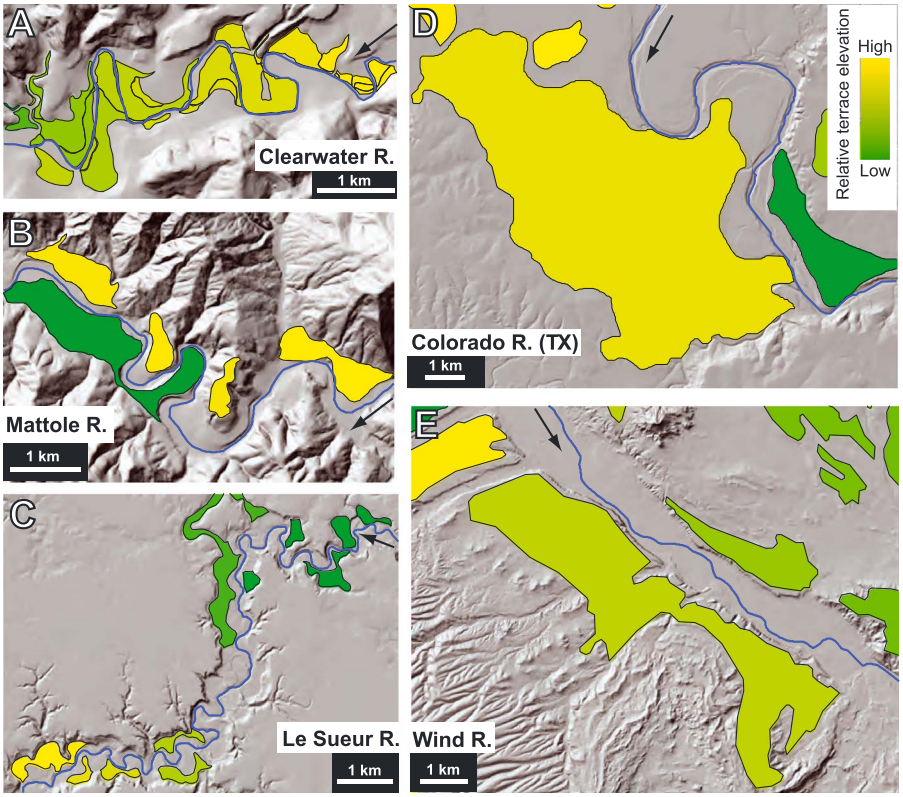

Figure 1. A variety of river terrace morphologies. Topographic shaded relief is overlain by previously mapped terrace extents. Arrows indicate flow direction. Mean terrace elevation is measured relative to the closest point on the longitudinal profile (green-yellow shading), and the range of mean terrace elevations is noted below. (a) The Clearwater River, Washington (47.6°N, 124.2°W; mapped by *Wegmann and Pazzaglia* [2002]; range in mean terrace elevation is 48 m). (b) The Mattole River, California (40.2°N, 124.2°W; mapped by *Dibblee and Minch* [2008]; range in mean terrace elevation is 104 m). (c) The Le Sueur River, Minnesota (44.0°N, 94.0°W; mapped by *Lusardi et al.* [2002]; range in mean terrace elevation is 9 m). (d) The Colorado River, Texas (30.2°N, 97.5°W; mapped by *Barnes et al.* [1974a, 1974b]; range in mean terrace elevation is 3 m). (e) The Wind River, Wyoming (42.3°N, 109.1°W; mapped by *Case et al.* [1998]; range in mean terrace elevation is 141 m). Topography data are from the National Elevation Dataset 1/3 arc sec digital elevation model (DEM; approximately 10 m grid spacing).

changes in water and sediment fluxes due to climate change [*Molnar et al.*, 1994; *Hancock and Anderson*, 2002; *Bridgland and Westaway*, 2008; *Pazzaglia*, 2013].

Evidence for terrace formation driven by climate change primarily relates to terrace age and geometry, although sedimentology of terrace fills is also used [*Tyráček et al.*, 2004; *Bridgland and Westaway*, 2008]. Terrace age is commonly compared to paleoclimate proxies [*van den Berg and van Hoof*, 2001; *Pan et al.*, 2003; *Picotti and Pazzaglia*, 2008; *Fuller et al.*, 2009], some of which record quasiperiodic variations such as Milankovitch cycles [*Hays et al.*, 1976]. Despite these important studies, relationships between terrace age and paleoclimate records are uncertain due to dating precision limits [e.g., *Wegmann and Pazzaglia*, 2002], and in the case of strath terraces uncertainty exists in the elapsed time between strath beveling and deposition of overlying alluvium [*Merritts et al.*, 1994]. In valleys where alluvial terraces have been argued to record climate cycles, there is commonly a discordance between the number of terrace levels and the number of inferred climate cycles [*Bridgland and Westaway*, 2008]. A variety of terrace geometric properties are commonly considered in order to interpret terrace origin and infer channel kinematics. These properties include terrace slope [e.g., *Merritts et al.*, 1994; *Finnegan and Dietrich*, 2011], terrace occurrence at similar elevation on opposite sides of a channel (i.e., pairing) [*Merritts et al.*, 1994], terrace width [*Lavé and Avouac*, 2001], and terrace length [*Wegmann and Pazzaglia*, 2002]. Terrace geometries attributed to climate change include pairing [*Wegmann and Pazzaglia*, 2002] and along-valley continuity [*Pazzaglia et al.*, 1998], following conceptual models that predict long periods of river longitudinal profile stability and strath beveling punctuated by vertical incision and terrace abandonment [*Hancock and Anderson*, 2002].

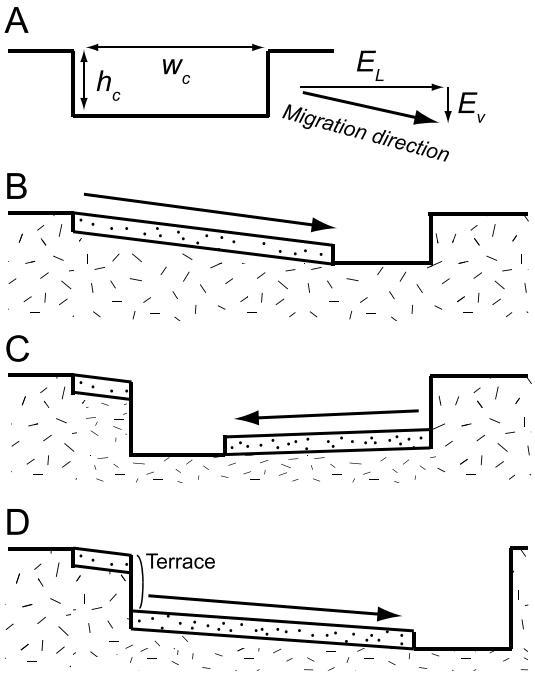

Figure 2. Schematic of river terrace formation by vertical erosion and a switching direction of lateral erosion [after *Merritts et al.*, 1994]. (a) The cross section of a channel with width w_c and depth h_c. The channel migrates with a constant lateral erosion rate (E_L) and constant vertical erosion rate (E_V), resulting in a subhorizontal channel migration direction. (b) As the channel erodes laterally and vertically, it planes off a bedrock (hatched area) surface. Here constant channel width is maintained by emplacing sediment (dotted area) on the trailing bank up to the flow depth. The arrow indicates the mean channel migration direction. (c) The direction of net lateral channel migration switches. (d) The direction of net lateral channel migration reverts to its initial direction. A strath terrace is preserved because the channel does not sweep a consistent distance across the valley. The same model holds for formation of an alluvial cut terrace.

Climatic and tectonic signals that would imprint the landscape must pass the filter of surface processes [*Schumm*, 1977; *Bull*, 1991; *Jerolmack and Paola*, 2010; *Ganti et al.*, 2014]. The terrace record of climate and tectonic change in particular is complicated by terrace erosion [*Lewin and Macklin*, 2003] and overprinted by autogenic terraces. For example, *Finnegan and Dietrich* [2011] showed that if vertical erosion rate is proportional to channel slope, then meander bend growth and cutoff should cause abrupt changes in channel slope (i.e., knickpoints) that propagate upstream and cause pulses of vertical incision that abandon terraces. For meandering streams, lateral erosion rates inherently vary in space and time as meander bends migrate and cut off and as the channel belt wanders across the valley [*Brice*, 1974; *Howard and Knutson*, 1984; *Seminara*, 2006]. *Davis* [1909] hypothesized that a vertically incising, laterally migrating channel (Figure 2a) can abandon terraces when it migrates in one direction (Figure 2b) before switching direction and migrating back toward its starting point (Figure 2c). Because the channel is incising vertically, the terrace riser is formed by lateral erosion of the cutbank (Figure 2c) and the terrace is fully abandoned when the channel changes direction once more (Figure 2d). This mechanism has been observed to drive terrace formation in experimental alluvial fans [*Mizutani*, 1998] and in field settings where engineered base level fall has induced rapid vertical incision [*Born and Ritter*, 1970; *Ben Moshe et al.*, 2008]. Although a switching direction of channel migration is rarely considered as a mechanism for forming alluvial or strath terraces [*Challinor*, 1932; *Hack*, 1955; *Stricklin*, 1961; *Merritts et al.*, 1994; *Erkens et al.*, 2009], numerical model results indicate that meandering can generate strath terraces even under constant rates of vertical incision [*Limaye and Lamb*, 2014].

Several characteristics have been attributed to terraces formed by unsteady channel migration, including a terrace slope equal to the ratio vertical-to-lateral erosion rate [*Merritts et al.*, 1994], a terrace dip direction oriented toward the valley center [*Davis*, 1909; *Merritts et al.*, 1994], a lack of corresponding terraces across the valley (i.e., unpaired) [*Bull*, 1990; *Merritts et al.*, 1994; *Wegmann and Pazzaglia*, 2002], and limited terrace length along valley [*Pazzaglia et al.*, 1998; *Pazzaglia*, 2013]. However, none of these terrace properties has been verified through direct field observations, numerical modeling, or experiments except for those of *Mizutani* [1998], who noted that laterally migrating, vertically incising channels formed surfaces that slope inward toward the channel.

The sparsest requirement to generate terraces is a lateral erosion rate that varies in space or time, as occurs for all meandering rivers, and a finite rate of vertical incision [*Davis*, 1909]. In principle, this basic terrace formation mechanism should be possible in all environments, including valleys with alluvial or strath terraces. Importantly, unlike terrace generation by external drivers such as climate change [*Hancock and Anderson*, 2002], this mechanism of autogenic terrace formation does not require the vertical incision rate to oscillate in time and therefore serves as an important null hypothesis before adopting models that require more complex erosion histories.

Herein we use a numerical model to isolate the expected age distribution and geometry of autogenic terraces formed by a meandering river undergoing steady vertical incision. In section 2, we describe our specific hypotheses, identify important variables, and use the field cases in Figure 1 for guidance on model parameterization. In section 3, we describe the methods used for modeling channel migration and identifying modeled terraces automatically. Section 4 presents the model results, including the variety of surface morphologies formed by the meandering model. We analyze terrace age and geometry across a broad range of channel lateral and vertical erosion rates and also consider cases in which variable bank strength and pulses of vertical incision influence terrace formation. In section 5 we compare model results to the case examples given in Figure 1. We discuss implications for inferring terrace origin in section 6.

2. Hypotheses and Field Examples

Meander bends have characteristic length scales [*Williams*, 1986] and migration patterns [*Hooke*, 2013]. Consequently, we hypothesize that terraces generated by meandering with constant vertical incision have characteristic geometries and age distributions that might set them apart from terraces driven by pulses of vertical incision. Model runs suggest that in bedrock river valleys, differences in bank strength between alluvial sediments and bedrock can explain a variety of valley morphologies and promote unsteady lateral channel migration and terrace formation [*Limaye and Lamb*, 2014]. Therefore, we also hypothesize that evolving bank strength differences alter the age and geometry of terraces generated by meandering with constant vertical incision.

2.1. Key Variables

We seek to determine the characteristics of terraces—including the time between unique terrace levels ($\Delta t_{terrace}$), maximum terrace length ($L_{terrace,max}$), terrace surface slope ($S_{terrace}$), terrace dip direction ($\varnothing_{terrace}$), and pairing fraction (f_{paired})—formed by meandering rivers with constant vertical incision and in a general way for both alluvial and strath terraces. Following *Limaye and Lamb* [2014], eight parameters can describe the kinematics of valley evolution for a mixed bedrock-alluvial meandering channel: the maximum lateral erosion rate in bedrock (E_{Lb}) and sediment (E_{Ls}), vertical incision rate (E_v), channel width (w_c), initial alluvial belt width (w_{ab}) and unconfined alluvial belt width (w_{uab}), channel depth (h_c), and the total simulation time (t) (Table A1). These eight parameters are chosen for the sparsest representation of valley evolution by a river channel with explicitly resolved dimensions that incises vertically and migrates laterally in sediment and/or bedrock banks.

Several factors may influence vertical incision rates, lateral erosion rates, and terrace formation, including sediment supply [*Sklar and Dietrich*, 2001], channel slope [*Stark*, 2006; *Finnegan and Dietrich*, 2011], uplift rate [*Lavé and Avouac*, 2001; *Amos and Burbank*, 2007; *Yanites and Tucker*, 2010], discharge variability [*Turowski et al*., 2008; *Stark et al*., 2010], channel substrate [*Ferguson*, 1973; *Finnegan et al*., 2005], tributaries [*Gutierrez et al*., 2014], and hillslopes [*Langston et al*., 2015]. In addition, valley widening may be carried out by braided rather than meandering channels [*Ryder and Church*, 1986; *Finnegan and Balco*, 2013]. Vertical and lateral erosion rates also may not be independent [e.g., *Finnegan and Dietrich*, 2011]. Herein we do not treat these processes explicitly so that the vertical incision and lateral erosion rates can be treated as the independent variables and varied over a wide parameter space.

Using dimensional analysis, the model parameters can be recast as independent nondimensional parameters. For equal, maximum rates of lateral erosion (E_L) in sediment and bedrock (i.e., $E_L = E_{Ls} = E_{Lb}$), these parameters include the dimensionless simulation time

$$t^* = \frac{E_L t}{w_c}, \tag{1a}$$

the dimensionless vertical incision rate

$$E_V^* = \frac{E_V w_c}{E_L h_c}, \tag{1b}$$

the channel width-to-depth ratio

$$w_c^* = \frac{w_c}{h_c}, \tag{1c}$$

and the dimensionless initial alluvial belt width

$$w_{ab}^* = \frac{w_{ab}}{w_{uab}} \tag{1d}$$

that describes the initial width of a sediment-filled zone, one channel depth thick, with respect to the estimated meander belt width for an unconfined case. As shown by *Limaye and Lamb* [2014], the model results for cases with variable bank material are strongly influenced by initial conditions, which is why w_{ab}^* must be considered as a variable.

A single variable for maximum lateral erosion rate in equations (1a) and (1b) is sufficient for evolution of a valley with banks of similar material, such as the Colorado River (Figure 1d), where the banks are mostly alluvium, or the San Juan River, Utah, where the banks are mostly bedrock [*Limaye and Lamb*, 2014]. However, in cases where differences in the strength of bank material (e.g., mixed bedrock and alluvial banks) influence valley evolution [*Limaye and Lamb*, 2013, 2014], we distinguish between two different lateral erosion rates for the two materials. Therefore, for these cases equation (1b) can be replaced by

$$E_{Vb}^* = \frac{E_V w_c}{E_{Lb} h_c} \tag{2a}$$

and in sediment

$$E_{Vs}^* = \frac{E_V w_c}{E_{Ls} h_c} \tag{2b}$$

where E_{Lb} and E_{Ls} are the maximum lateral erosion rates in bedrock and sediment, respectively. For cases with variable bank strength, t^* (equation (1a)) is defined using the lateral erosion rate in sediment banks.

Previous model runs suggested that the nondimensional vertical incision rate, which reflects the ratio of vertical-to-lateral erosion rate (equation (1b)), strongly influences the large-scale valley geometry excavated by the river. Specifically, high values of the dimensionless vertical incision rate favor the formation of deep, narrow gorges rather than terraced valleys, and low nondimensional vertical incision rates favor broad, low-relief valleys with the potential for terraces [*Limaye and Lamb*, 2014]. Based on these results, we hypothesize that the nondimensional vertical incision rate (E_V^*) also controls the age distribution and geometry of terraces formed during valley excavation. We also hypothesize that nondimensional simulation time (t^*) influences the age and geometry of preserved terraces because more extensive lateral channel migration erodes existing landforms. Field data sufficient to test these hypotheses are rare, but *Lewin and Macklin* [2003] identified alluvial deposits consistent with selective preservation, and numerical modeling results suggest that the distribution of floodplain sediment ages generated by meandering reflects preferential preservation of older sediments [*Bradley and Tucker*, 2013]. To test these specific hypotheses, we performed a suite of model runs in which we separately varied t^* and E_V^* while holding the other dimensionless variables constant.

Under the assumption of uniform bank materials, the dimensionless alluvial belt width, w_{ab}^*, is irrelevant because w_{ab} only influences channel migration if lateral erosion rates differ in sediment and bedrock [*Limaye and Lamb*, 2014]. For cases with differences in bank strength between sediment and bedrock, we hypothesize that this contrast alters spatial patterns of channel migration and consequently influences terrace age and geometry. Thus, to test this hypothesis, we used the model to systematically explore the time interval between terrace levels and terrace geometry as a function of dimensionless vertical incision rate for bedrock banks (E_{Vb}^*) while holding w_c^*, t^*, w_{ab}^*, and E_{Vs}^* constant.

Finally, we are interested in whether autogenic terraces can be distinguished from those formed from externally driven pulses of vertical incision when both mechanisms are operating simultaneously. We hypothesize that river lateral erosion removes terraces produced by pulses of vertical incision and overprints the valley with autogenic terraces. Using the model, we test these ideas by comparing model runs under constant vertical incision to cases where vertical incision occurs in discrete pulses.

2.2. Example Field Cases

We use the natural river valleys introduced in Figure 1 to guide selection of a realistic range for the model variables in equations (1a)–(1d) and to compare to the model results in section 5. The natural river valleys serve as a representative, but not exhaustive, compilation. We choose these valleys because they are well

Table 1. Estimated Parameters for Rivers Shown in Figure 1 and the San Juan River[a]

Valley Name	Location	w_c (m)	h_c (m)	E_L (mm/yr)	E_V (mm/yr)	E_V^*	$t_{vert} = \Delta z/E_V$ (year)
San Juan	37.2°N, 109.9°W	53[b]	2.7[c]	3 ± 1.5[d,e]	0.16 ± 0.05[f]	1.07 (0.49, 2.80)	6700 (5000, 10,000)
Mattole	40.2°N, 124.2°W	102[b]	5.1[c]	28.5 ± 10.5[g]	1.25 ± 0.55[h]	0.88 (0.61, 1.45)	800 (550, 1430)
Colorado	30.2°N, 97.5°W	275[i]	8.0[i]	150 ± 75[e,j]	0.29 ± 0.04[j]	0.07 (0.04, 0.15)	3450 (3030, 4000)
Wind	43.4°N, 109.3°W	41.7[k]	1.8[i]	10 ± 5[l,e]	0.15 ± 0.01[m]	0.35 (0.22, 0.74)	6700 (6250, 7140)
Le Sueur	43.9°N, 94.1°W	47.5[n]	2.4[c]	300 ± 200[n]	1.6 ± 0.4[n]	0.11 (0.05, 0.40)	630 (500, 830)
Clearwater[o]	47.7°N, 124.2°W	49.1[b]	2.5[c]	375 ± 187[e,p]	0.8 ± 0.4[p]	0.04 (0.01, 0.13)	1250 (830, 2500)

[a]Values in parentheses indicate estimated lower and upper bounds.
[b]Estimated from aerial photographs.
[c]Estimated assuming $w_c/h_c = 20$.
[d]Estimated for a mean lateral erosion rate in bedrock of 1 mm/yr, approximately 1 order of magnitude slower than in more erodible sedimentary rock [*Montgomery*, 2004].
[e]Uncertainty estimated as 50%.
[f]Estimated from *Wolkowinsky and Granger* [2004] and *Hanks and Finkel* [2005].
[g]Estimated from bedrock lateral erosion rates in similar geologic environments by *Fuller et al.* [2009] and *Finnegan and Dietrich* [2011].
[h]Estimated from *Merritts et al.* [1994].
[i]*Blum* [1992].
[j]Estimated from stratigraphic data from *Blum and Valastro* [1994] (see Figure 7 in that study).
[k]*Smalley et al.* [1994].
[l]Based on estimate by *Hancock and Anderson* [2002].
[m]Estimated from *Chadwick et al.* [1997].
[n]Estimated from *Gran et al.* [2011].
[o]Terrace analysis restricted to strath terraces Q_{t4}, Q_{t5}, and Q_{t6} in *Wegmann and Pazzaglia* [2002].
[p]Estimated from *Wegmann and Pazzaglia* [2002].

studied, have terrace age constraints, and span a wide range in terrace sizes and geometries (Figure 1), rock types, tectonic settings, erosion rates, and hypothesized terrace formation mechanisms. For example, the valleys of three rivers—the Clearwater (Figure 1a), Colorado (Figure 1d), and Wind Rivers (Figure 1e)—have terraces interpreted to record a history of unsteady vertical incision driven by climate change [*Blum and Valastro*, 1994; *Hancock and Anderson*, 2002; *Wegmann and Pazzaglia*, 2002]. In contrast, strath terraces in the Mattole River valley (Figure 1b) are thought to form by steady vertical incision and unsteady lateral erosion [*Merritts et al.*, 1994]. The Le Sueur River, Minnesota (Figure 1c), is known to have undergone pulses of vertical incision caused by a series of propagating knickpoints that generated numerous terraces [*Gran et al.*, 2013]. The San Juan River valley serves as an example with limited terrace development.

To estimate the appropriate dimensionless variables for the field examples, we use existing literature to constrain lateral and vertical incision rates and channel dimensions (Table 1). When not reported in previous work, we estimated channel dimensions based on aerial images (Table 1). Most estimates of lateral erosion rates discussed below are temporal averages, whereas our model results are cast in terms of maximum lateral erosion rates (as discussed in section 3.1). Therefore, we estimate and report in Table 1 the maximum lateral erosion rate as 3 times the average, based on results from the *Howard and Knutson* [1984] meandering model.

For the Clearwater River, *Wegmann and Pazzaglia* [2002] estimated an average lateral erosion rate of 125 mm/yr based on the width of their Q_{t5} strath terrace. Based on radiocarbon dates of strath terrace alluvium in the reach 15 to 30 km upstream from the river mouth [*Wegmann and Pazzaglia*, 2002], we compute a mean vertical incision rate of $E_V = 0.8 \pm 0.4$ mm/yr. Radiocarbon dating on the Mattole River terraces constrains vertical incision rate to 0.7 to 1.8 mm/yr over the last 12 kyr [*Merritts et al.*, 1994]. We estimate the maximum lateral erosion rate as ranging from 28.5 ± 10.5 mm/yr based on two estimates of average lateral erosion rates for similar rivers in the region (Eel River [*Fuller et al.*, 2009] and Smith River [*Finnegan and Dietrich*, 2011]). For the Colorado River, we use radiocarbon dates from *Blum and Valastro* [1994] (see Figure 7 of that study) to estimate an average lateral erosion rate and convert this to a maximum lateral erosion rate of 150 ± 75 mm/yr. Using the same age data and terrace elevations, we estimate a vertical incision rate of 0.29 ± 0.04 mm/yr. For the Wind River, the average vertical incision rate between the WR-7 and WR-3 strath-capping gravels near Riverton, WY, is 0.15 ± 0.01 mm/yr [*Chadwick et al.*, 1997], and the maximum lateral erosion rate is estimated as 10 ± 5 mm/yr using the average lateral erosion rate estimated by *Hancock and Anderson* [2002]. For the Le Sueur River, the average vertical incision rate is 1.6 ± 0.4 mm/yr since 13 ka, and the maximum lateral erosion rate is measured historically as 300 ± 200 mm/yr [*Gran et al.*, 2011]. Cosmogenic radionuclide dating of perched

gravels in the San Juan River valley indicates an average vertical incision rate of 0.16 ± 0.05 mm/yr since 1.36 Ma [*Wolkowinsky and Granger*, 2004; *Hanks and Finkel*, 2005]. The banks of the San Juan River are commonly composed of highly resistant sandstone [*Harden*, 1990], and we estimate a maximum lateral erosion rate 3 ± 1.5 mm/yr based on comparison to rates in weaker rocks elsewhere [*Montgomery*, 2004]. Together, we find a range of values for E_v^* from 0.04 (Clearwater River) to 1.07 (San Juan River) (Table 1).

3. Model Formulation and Methods

It is difficult to test our hypotheses with existing terrace models because most do not include meandering [*Veldkamp and van Dijke*, 2000; *Hancock and Anderson*, 2002; *Finnegan*, 2013; *Langston et al*., 2015] or do not represent spatial differences in bank strength within valleys [*Veldkamp and van Dijke*, 2000; *Hancock and Anderson*, 2002; *Finnegan and Dietrich*, 2011]. Models that do include meandering have not systematically analyzed the age and geometry of simulated terraces [*Lancaster*, 1998; *Finnegan and Dietrich*, 2011; *Limaye and Lamb*, 2014]. In contrast to previous studies that have primarily compared terrace age to paleoclimate proxies without explicitly considering channel kinematics [*Pan et al*., 2003; *Bridgland and Westaway*, 2008; *Fuller et al*., 2009], we use a forward modeling approach with constant boundary conditions to explicitly test how channel vertical and lateral erosion rates influence terrace generation.

We follow the approach of *Limaye and Lamb* [2014] to simulate river valley evolution. We use the simplest possible numerical model that incorporates river meandering and vertical incision and tracks differences in bank strength between bedrock and sediment. To limit the computational intensity of the model runs and permit modeling of terrace evolution over timescales of 100,000 years, we employ a relatively simple and commonly used model of river meandering in which channel curvature drives bend migration [*Howard and Knutson*, 1984]. This model reproduces key meandering kinematics and geometries, including growth, downstream translation, and asymmetry of meander bends [*Howard and Knutson*, 1984]. Known model limitations apply primarily to channel dynamics on timescales shorter than the cutoff timescale, including simplistic representation of hydrodynamics and sediment transport [*Seminara*, 2006], fixed channel width [*Parker et al*., 2011], the inability to generate compound bend shapes prior to cutoff [*Lancaster and Bras*, 2002] and other higher-order moments of channel migration [*Guneralp and Marston*, 2012], and higher sinuosity and regularity of meander bends than for natural cases [*Howard and Hemberger*, 1991]. These deficiencies are at least partially mitigated over timescales longer than the cutoff timescale because the step change in channel planform geometry appears to dominate hydrodynamic effects [*Camporeale et al*., 2005], cutoffs greatly increase the variety of bend shapes, and alluvial meandering channels tend to maintain channel width despite short-term differences in bank movement [*Parker et al*., 2011; *Eke et al*., 2014].

3.1. Meandering and Landscape Evolution Model

In the centerline evolution model [*Howard and Knutson*, 1984], local lateral erosion rate is a function of local and upstream-integrated curvature

$$R_1(s) = \Omega R_o(s) + \frac{\Gamma \int_0^{\xi_{\max}} R_o(s-\xi) G(\xi) \mathrm{d}\xi}{\int_0^{\xi_{\max}} G(\xi) \mathrm{d}\xi} \tag{3}$$

where R_1 is the dimensionless lateral erosion rate, s is the centerline node index, ξ is the along-channel distance, and $R_o = (r/w_c)^{-1}$, where r is the radius of curvature of the centerline at node s. The sign of R_o is set as positive where the local channel path is in the clockwise direction and negative where the path is counterclockwise. Ω and Γ are dimensionless parameters set to -1 and 2.5, respectively, and determine the relative weight of local (Ω) and upstream (Γ) curvature [*Ikeda et al*., 1981]. G is a weighting function

$$G(\xi) = e^{-\left(\frac{2kC_f}{h_c}\right)\xi} \tag{4}$$

with dimensionless scaling coefficient $k = 1$ [*Ikeda et al*., 1981]. C_f is a dimensionless friction coefficient set to 0.01, following *Stølum* [1996]. The maximum upstream distance for the integration of channel curvature is $\xi_{\max}$, where the normalized value of the weighting function falls below 1%. The local, dimensional lateral migration rate at centerline node s is

$$M(s) = k_e R_1(s) \mu^{\varepsilon} \tag{5}$$

where k_e is the lateral erosion rate constant, μ is average channel sinuosity, and ε is a dimensionless parameter set to $-2/3$ [*Howard and Knutson*, 1984].

The channel cross section is rectangular, where the channel width and depth are the bankfull values. A 2 year time step is used and represents the recurrence interval of the bankfull discharge typical for alluvial rivers [*Leopold et al.*, 1964]. Given uncertainties in the formative discharge for bedrock streams [*Tinkler and Wohl*, 1998; *Whipple*, 2004], the same time step is used for all model runs. Neck cutoffs are identified where channel banks connect with themselves; chute cutoffs are not modeled [e.g., *Sun et al.*, 1996; *Lancaster*, 1998; *Finnegan and Dietrich*, 2011]; and overbank deposition is implicitly assumed to fill meander loops immediately following cutoff [e.g., *Sun et al.*, 1996; *Finnegan and Dietrich*, 2011]. The model domain is arbitrarily large in the cross-valley direction and periodic in the along-valley direction, which permits the channel belt axis to wander freely. The along-valley length of the model domain is set to 120 channel widths or approximately 10 meander wavelengths [*Leopold and Wolman*, 1960]. The initial topography is a flat plane with the channel inset one channel depth.

The initial channel sinuosity is established by evolving an initially straight channel seeded with random, meter-scale noise for a fixed dimensionless simulation time $t^* = 500$ [*Limaye and Lamb*, 2014]. During this initialization phase, channel bends grow and develop past the point of cutoff so that the initial random noise configuration is no longer apparent. At the end of the initialization phase, the erodibility coefficient k_e is set so that the maximum lateral migration rate of any channel centerline node equals E_L, i.e.,

$$k_e = \frac{E_L}{R_{1,\max}\mu^{\varepsilon}} \tag{6}$$

In simulations with bank strength differences between bedrock and sediment, equation (6) is replaced by

$$k_b = \frac{E_{Lb}}{R_{1,\max}\mu^{\varepsilon}} \tag{7a}$$

and for sediment

$$k_s = \frac{E_{Ls}}{R_{1,\max}\mu^{\varepsilon}} \tag{7b}$$

where k_b is the lateral erosion rate coefficient for all bedrock banks and k_s is the corresponding coefficient for all sediment banks.

Models with spatial variations in bank strength yield predictions for meandering channel trajectories that are generally sensitive to grid resolution except in cases of large channel migration rates [*Limaye and Lamb*, 2013]. Therefore, we couple the centerline evolution model to the vector-based method of *Limaye and Lamb* [2013] for tracking bank materials, which does not use grids. We track two classes of material that can be assigned distinct erodibilities: bedrock and sediment. The local erosion rate coefficient is scaled according to the fraction of bank material that is bedrock (f_b), measured from the channel bed to the bankfull height

$$k_e = k_s(1 - f_b) + k_b f_b \tag{8}$$

Fluxes of water and sediment are not explicitly tracked; sediment is automatically emplaced along the trailing bank as the channel migrates across the valley, with a thickness equal to the channel depth (Figure 2). Similarly, eroded sediment is automatically removed from the model domain, except for that emplaced on the trailing edge of the channel. When the channel erodes laterally, it removes the entire vertical column of material that it encounters (Movies S1–S7 in the supporting information, which are further discussed in section 4).

We seek to explore terrace formation under simplified scenarios where we can isolate and impose vertical incision rate as a constant (equation (1b)). This assumption introduces a complication because channel slope evolves in natural meandering channels as meander bends grow and suddenly shorten through cutoffs [*Hooke*, 2013], and slope has been hypothesized to influence vertical incision rates [*Howard and Kerby*, 1983; *Stark*, 2006; *Finnegan and Dietrich*, 2011]. If vertical incision rates were fixed, then knickpoints formed by meander cutoff would neither propagate nor diffuse [*Seidl and Dietrich*, 1992] and would constitute an increasing proportion of the channel longitudinal profile. In order to isolate the role of unsteady lateral erosion without introducing a variety of unconstrained knickpoint processes, we follow *Limaye and Lamb* [2014]

Table 2. Terrace Detection Parameters for Simulated Topography

Parameter	Value
Threshold local relief	1 m
Local relief window	30 m by 30 m
Minimum elevation above top of channel	h_c
Threshold terrace area	100 m^2
Threshold mean terrace width	$2w_c$
Maximum difference in mean elevation for paired terraces	2 m
Threshold elevation difference for separation into unique terrace levels	1 m

and set channel slope to zero to prevent slope evolution, and vertical incision rate is varied as an independent parameter. Thus, model behavior should most closely approximate natural streams with low slopes.

3.2. Terrace Detection

3.2.1. Simulated Terraces

Each model run generates vector data for valley and channel evolution [*Limaye and Lamb*, 2013]. These vector data are converted to gridded surface age, surface topography, and bedrock topography using a 10 m grid spacing similar to field-scale digital elevation models (DEMs) [e.g., *Gesch*, 2007]. These grids are used for statistical comparison of terrace attributes. To map simulated terraces objectively and rapidly, we use a new algorithm to identify terraces that is closely related to previous work [*Demoulin et al*., 2007; *Stout and Belmont*, 2013]. The algorithm reflects common methods used for mapping terraces based on gradients in digital elevation models [*Fuller et al*., 2009; *Gran et al*., 2011] and for classifying terraces based on spatial relationships to other landscape features, including the modern river channel and other terraces [*Merritts et al*., 1994]. Terrace identification metrics are summarized in Table 2.

Terrace surfaces are identified as groups of contiguous DEM pixels that meet criteria for local relief ($<$1 m) and elevation relative to the channel ($>$1 channel depth above the top of the channel). We measure local relief as the standard deviation of elevation over a fixed, 30 m by 30 m window centered on each DEM pixel. This window geometry is similar to that used in field cases using DEMs [*Burrough and McDonell*, 1998; *Gesch*, 2007]. The local relief threshold is chosen to approximate the minimum difference in elevation commonly used to differentiate terrace tread elevations (i.e., Δz) [*Personius*, 1995; *van den Berg*, 1996; *Wegmann and Pazzaglia*, 2002; *Gran et al*., 2013]. Qualitatively, the same relief threshold differentiates most low-relief terrace treads from high-relief terrace risers in DEMs of natural landscapes. In addition, a threshold area is applied to reduce spurious terrace detections; the threshold is set at 100 m^2 following *Fuller et al*. [2009], which is a typical pixel area in field-scale DEMs [e.g., *Gesch*, 2007]. We only consider terraces that are wider than two channel widths, and thus effectively remove misidentified cutoff loops from the terrace database.

The remaining terrace objects are analyzed further for mean surface elevation, age (for model runs), slope, dip direction, area, and length (Table A1). We define terrace length as the maximum distance spanned by the terrace parallel to the mean valley direction and nondimensionalize terrace length by channel width. For natural terraces, individual surfaces may be diachronous because of longitudinal differences in abandonment time, for example, due to spatially variable sediment evacuation [*Weldon*, 1986] or knickpoint propagation [*Finnegan*, 2013]. These factors are not included in the model, and, in general, the model topography does not exhibit systematic, streamwise trends in surface age.

We identify paired terraces in the model runs automatically and objectively. A rectangular bounding box is fit to each individual terrace, and a search window with a width equal to the width of the terrace is constructed by extending the bounding box in the across-valley direction. The local valley azimuth is determined by smoothing the local channel centerline. If the search window overlaps a terrace on the other side of the active channel and if the mean terrace elevations with respect to the local channel elevation differ by less than a threshold value, then the terraces are flagged as paired. Considering the threshold local relief for terrace riser definition (1 m over a 30 m baseline) and the range of terrace widths (commonly tens to hundreds of meters), a single terrace tread can span several meters in elevation. Therefore, we identify terraces with mean elevations within 2 m of each other as paired. This pairing criterion is relatively conservative because terraces with overlapping elevation ranges are classified as unpaired if the difference in mean terrace elevation exceeds 2 m or if terraces are separated along the valley. We calculate the fraction of paired terraces (f_{paired}) that form in our model runs and weight the results by terrace area.

Commonly, terrace surfaces in a given catchment are grouped into unique levels according to their elevation with respect to the channel [*Baker and Penteado-Orellana*, 1977; *Wegmann and Pazzaglia*, 2002; *Fuller et al*., 2009], which along with sedimentologic characteristics and ages [*Baker and Penteado-Orellana*, 1977; *Blum and Valastro*, 1994; *Bridgland and Westaway*, 2008; *Wegmann and Pazzaglia*, 2009] are used to identify surfaces formed at similar times and by similar processes. Because elevation is more readily measured than material can be dated, it is rare for each terrace surface to be independently dated [e.g., *Fuller et al*., 2009]. Therefore, in order to identify the number of unique terrace levels in a way consistent with many field studies, we classify terraces as belonging to the same level if their mean elevations fall within the same elevation bin. The elevation bin height (Δz) is set at 1 m, consistent with reported variations of strath elevation and minimum differences in terrace elevation [*Personius*, 1995; *van den Berg*, 1996; *Wegmann and Pazzaglia*, 2002; *Gran et al*., 2013]. The distribution of time intervals between unique terrace levels ($\Delta t_{terrace}$) is calculated by sorting the unique terrace levels by mean surface age then differencing these ages. Unless otherwise noted, we analyze the median value ($\Delta t_{terrace,50}$) of this distribution. We also report the tails of the terrace age distribution (i.e., 10th [$\Delta t_{terrace,10}$] and 90th [$\Delta t_{terrace,90}$] percentiles) to quantify whether the terraces have a repeating, characteristic time interval.

As will be shown in the results, the time interval between unique terrace levels ($\Delta t_{terrace}$) is most strongly controlled by the time for vertical incision to generate relief sufficient to define a unique terrace level

$$t_{vert} = \frac{\Delta z}{E_V} \tag{9}$$

In the analysis that follows, we nondimensionalize the characteristic terrace timescale $\Delta t_{terrace}$ by t_{vert}, which allows us to explore secondary controls on $\Delta t_{terrace}$ apart from the vertical incision rate and the elevation threshold Δz. Results presented in this framework are less sensitive to the particular threshold Δz for terrace differentiation. Thus, $\Delta t_{terrace,50}/t_{vert} = 1$ corresponds to the shortest median time interval between terraces allowed by the model setup.

3.2.2. Natural Cases

For natural landscapes, erosion, hillslope processes, and other landscape features (e.g., roads) complicate accurate terrace detection [e.g., *Stout and Belmont*, 2013], and field-based observations are often needed for correct identification [*Merritts et al*., 1994; *Bridgland and Westaway*, 2008; *Wegmann and Pazzaglia*, 2009]. Therefore, we extracted terrace tread extents from geologic maps (partially shown in Figure 1). In our modeling, which does not incorporate along-channel slope, all elevations are measured with respect to the spatially uniform elevation of the channel. Therefore, in order to measure natural DEM elevations within a reference frame consistent with the model runs, for each natural DEM pixel we subtract the elevation of the channel at the nearest point along the channel planform trace. This elevation correction is used to calculate terrace attributes including mean elevation, slope, dip direction, and pairing fraction but does not affect the planform terrace properties of length and area.

To compare the characteristic timescales of autogenic terraces with those for our field cases, we extract the mean elevation of terraces mapped for the valleys in Figure 1. We calculate the median elevation difference between unique terrace levels in the same manner used for the simulated terraces. The terrace elevations are translated to a median time difference between terrace levels ($\Delta t_{terrace,50}$) using the average vertical incision rate at each site (Table 1) and

$$\Delta t_{terrace} = \frac{\Delta z_{50}}{E_V} \tag{10}$$

where Δz_{50} is the median elevation difference between unique terrace levels. Similarly, the timescale for relief generation sufficient to abandon a terrace (t_{vert}) is estimated for each valley following equation (9). These calculations assume a constant vertical incision rate for comparison purposes; unsteady vertical incision rates would yield different values of $\Delta t_{terrace,50}$ and t_{vert}.

3.3. Modeled Parameter Space

We analyze two sets of model runs: one with constant bank strength and the other with variable bank strength (Table 3). In both cases, the channel width-to-depth ratio (w_c*) is fixed at 20 in our model runs—a value within

Table 3. Model Run Parameters

Set of Model Runs	t^*	E_V^*	E_{Vs}^*	E_{Vb}^*	w_{ab}^*	Number of Model Runs
Constant bank strength	1–5000	0.002–200	NA	NA	NA	190[a]
Variable bank strength	5000	NA	0.002	0.004–4	0.1	21

[a]Each model run with a unique set of parameters was run 10 times, each time with a different initial channel planform geometry. NA: not applicable.

the range of mixed bedrock-alluvial channels [*Yanites and Tucker*, 2010] and alluvial meandering channels for moderate valley slopes [*Parker*, 1976]. The channel width and depth separately affect detailed model behavior; for example, depth affects meander wavelength, and width affects the threshold for neck cutoffs. In terms of dimensionless parameters, however, the channel aspect ratio only directly affects the dimensionless vertical incision rate (equation (1b)), so different channel aspect ratios can be accounted for through E_v^*. Though some strath terraces date to before 100 ka [*Pan et al.*, 2003], terraces are commonly dated as several or tens of thousands of years old [*Blum and Valastro*, 1994; *Merritts et al.*, 1994; *Fuller et al.*, 2009; *Gran et al.*, 2013]. Consequently, in our model runs we employ a maximum dimensional simulation time (t) of 100,000 years.

In the model runs with constant bank strength, we separately vary the nondimensional vertical incision rate (E_V^*) and the nondimensional simulation time (t^*) while holding the other parameters constant. We vary E_V^* from 0.002 to 200, representing a range of maximum lateral erosion rates from 1 mm/yr (i.e., highly resistant bedrock) to 1 m/yr (i.e., highly erodible floodplain sediments) and a range of dimensional vertical incision rates from 0.1 mm/yr (i.e., a slowly uplifting continental interior environment) to a high of 10 mm/yr (i.e., an active orogen) [*Montgomery*, 2004], which encompasses our field examples (Table 1). We vary t^* from 1 to 5000 (i.e., the time for the channel to migrate laterally 1 to 5000 channel widths in sediment bank materials).

The model runs with variable bank strength involve tracking the evolving spatial distribution of bedrock and sediment and thus are more computationally intensive [*Limaye and Lamb*, 2013]. Therefore, instead of an exhaustive exploration of model parameters for cases with variable bank strength, we focus our analysis on the effect of changing the strength of the bedrock banks. Therefore, we fix the nondimensional vertical incision rate for sediment banks ($E_{Vs}^* = 0.002$) and the nondimensional simulation time ($t^* = 5000$) and vary only E_{Vb}^*. The cases with variable bank strength involve an additional parameter, the nondimensional width of the initial alluvial belt (w_{ab}^*), due to erodibility differences between sediment and bedrock. In order to characterize the first-order influence of an alluvial belt with a finite initial width, we set $w_{ab}^* = 0.1$ (i.e., the channel is initially confined within a zone of sediment fill one channel depth in thickness, with bedrock at the lateral boundaries of the fill and at the channel bed). See *Limaye and Lamb* [2014] for model results that vary w_{ab}^*.

The kinematic evolution of simulated meandering channels is highly sensitive to initial planform geometry [*Frascati and Lanzoni*, 2010], which causes different patterns of erosion and terrace development for the same model parameters. Whereas previous model runs using an identical model formulation indicated that river valley aspect ratio is generally insensitive to initial channel planform geometry [*Limaye and Lamb*, 2014], river terraces exhibit a greater sensitivity to initial conditions because they are finer in scale. Consequently, we ran the model with constant bank strength and a unique set of parameters 10 separate times, each with a different initial channel planform geometry resulting from different planimetric noise during the initialization phase.

Terrace statistical distributions, including the time between terrace levels, and maximum terrace length, slope, dip direction, and pairing fraction are computed separately for each model run and then considered collectively for each set of parameters. We set $\Delta t_{terrace}$ as undefined when fewer than two terraces form for more than half of the model runs with the same parameters but different initial channel geometry. Because model runs that track differences in bank strength are more computationally intensive, only one run is conducted for each unique set of parameters in these cases. Therefore, the results presented for cases with variable bank strength do not account for the same variety of initial conditions as the cases with constant bank strength. The procedure for initially evolving the channel sinuosity is the same as in the model runs with constant bank strength, except that the channel is not allowed to erode laterally past bedrock boundaries during the initialization phase [*Limaye and Lamb*, 2014].

4. Model Predictions for Terrace Formation

In this section we present model results for terrace formation that are motivated by our hypotheses in section 2. We begin by describing terrace age and geometry for cases with constant vertical incision rates and constant bank strength. In section 4.2 we then consider the effects of variable bank strength on terrace formation and geometry. In section 4.3 we compare examples of terrace formation by pulsed and constant vertical incision rates.

4.1. Model Runs With Constant Bank Strength

Qualitatively, the model runs with constant bank strength and constant vertical incision rates generate three types of valleys, examples of which are shown in Figure 3. The large-scale geometry of the valley and the occurrence of terraces at smaller scales are sensitive to both t^*, which determines the amount of valley widening, and E_V^*, which determines the amount of valley deepening relative to valley widening [*Limaye and Lamb*, 2014].

In an example of the first valley type ($t^* = 5000$ and $E_V^* = 0.003$; Figure 3a and Movie S1 in the supporting information), channel lateral migration is extensive and vertical incision is slow compared to lateral erosion, so the channel erodes broad surfaces that are continuous along valley, similar to the Colorado River terraces (Figure 1d). The curves in the terrace margins and in the shaded relief indicate that the surfaces form by the growth of numerous meander bends that each erode a separate swath. Because of the relatively low vertical incision rate, the channel incises vertically only minimally between successive cycles of meander loop growth and cutoff. As a result, the surfaces eroded by the channel have similar elevations and thus contribute to forming the same terrace surface.

For an example of the second valley type ($t^* = 108$ and $E_V^* = 0.7$; Figure 3b and Movie S2 in the supporting information), channel lateral migration is also extensive, but the higher relative vertical incision rate impacts terrace properties in two ways. First, less area near the channel falls beneath the minimum elevation threshold for classification as a terrace, so terraces occur closer to the channel. Second, the terraces are smaller, more numerous, and bounded by individual meander cutoff loops, similar to the Clearwater River terraces (Figure 1a). This terrace geometry develops because under the relatively high vertical incision rate, the channel incises vertically a substantial amount between successive cycles of meander bend growth and cutoff. As a result, when the channel reoccupies a portion of the landscape, it commonly does so at a lower elevation and cuts a terrace riser (Figure 2c).

In an example of the third valley type ($t^* = 5$ and $E_V^* = 200$; Figure 3c), channel lateral migration is limited and greatly outpaced by vertical incision. All topography takes the form of slip-off surfaces and occasional meander cutoff loops, as is common for meanders deeply entrenched in bedrock (e.g., San Juan River) [*Harden*, 1990]. No terraces form because the surface slope, and thus local relief, is too high along the channel-eroded surfaces for them to be classified as terraces. We define this condition as "slope limited."

These examples illustrate that t^* and E_V^* strongly influence the number and geometry of river terraces formed by meandering with constant vertical incision. The combined influences of t^* and E_V^* are quantified in the following sections.

4.1.1. Terrace Age Distributions

Figure 4a shows the time interval between unique terrace levels ($\Delta t_{terrace,50}/t_{vert}$) as a function of t^* for several fixed values of E_V^* at which terrace formation is not slope limited. For increasing E_V^*, $\Delta t_{terrace,50}/t_{vert}$ is defined over a broader range of t^* because the channel generates more vertical relief, and potentially more terraces, for the same dimensionless simulation time. In general, terraces do not form at the margins of parameter space where different terrace definition thresholds are encountered. Slope-limited conditions prevail for relatively high nondimensional vertical incision rates ($E_V^* > 2$; Figure 4b) due to the local relief threshold (Table 2). Slip-off surfaces form instead, though they may be relatively narrow (Figure 3c). Terraces do not form for two additional reasons. First, relatively low dimensionless vertical incision rates do not generate sufficient relief for terrace formation (e.g., $E_V^* \leq 0.02$ for $t^* \leq 300$ in Figure 4a). We define this condition as "relief limited." Second, for relatively short dimensionless simulation times, lateral channel migration is insufficient to bevel a terrace surface (i.e., "migration limited," as for $t^* < 40$ in Figure 4a). Subsequent plots highlight regimes where terraces do not form for one or a combination of these reasons.

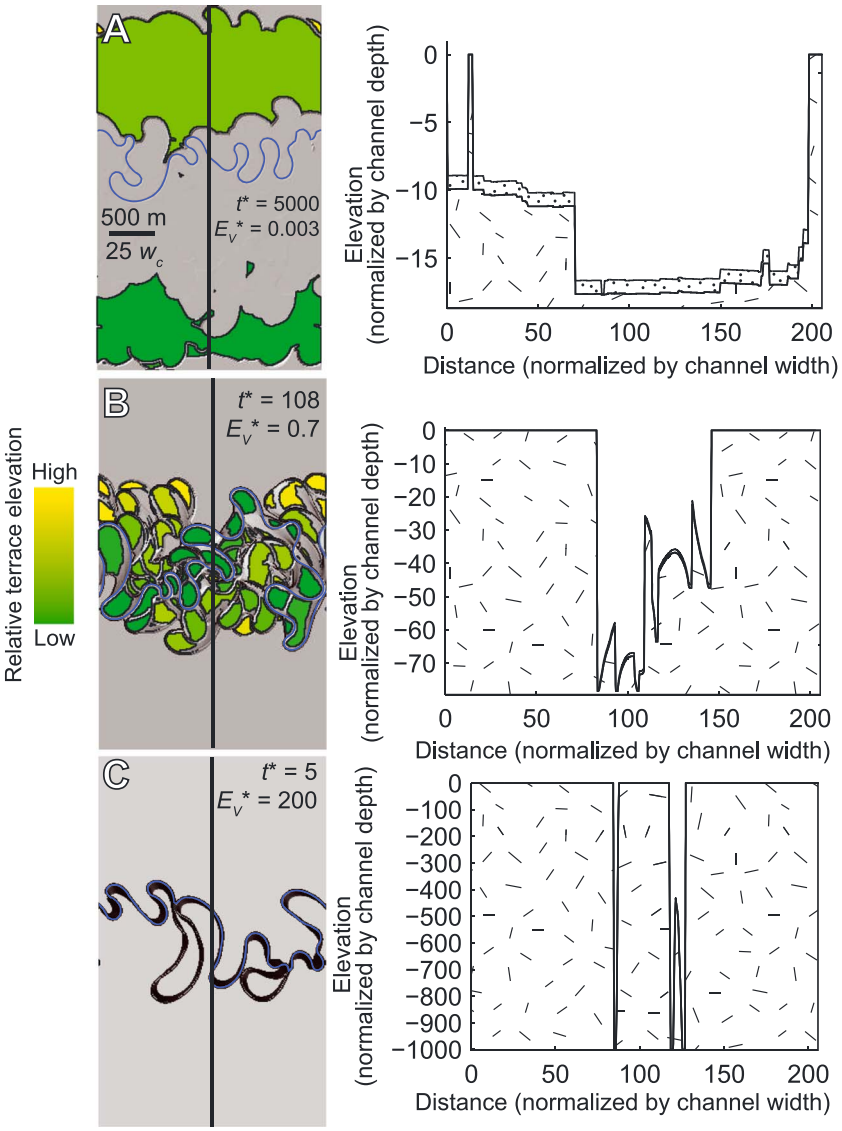

Figure 3. The surface morphologies produced by the model for constant bank strength, as a function of dimensionless simulation time (t^*) and dimensionless vertical incision rate (E_V^*). In each plan view panel, flow is from left to right, the channel is indicated in blue, the background is the shaded relief of topography, terraces are colored according to their mean elevation (green-yellow), and the thick black line indicates the location of the corresponding valley cross section that starts at the top of the model domain. The range of mean terrace elevations is noted below. The domain width is $120w_c$, and all map view panels have the same scale. At right, topographic cross sections indicate bedrock (hatched) and sediment (dotted). (a) For $t^* = 5000$ and $E_V^* = 0.003$, wide and long terraces form and represent composite surfaces eroded by numerous meander bends. Terrace elevation range is 15.3 m. (b) For $t^* = 108$ and $E_V^* = 0.7$, numerous terraces form and are generally bounded by abandoned meander cutoff loops. Terrace elevation range is 75 m. Sediment mantles terraces but is thin relative to the valley depth. (c) For $t^* = 5$ and $E_V^* = 200$, no terraces form because surfaces beveled by lateral channel erosion are exceedingly steep. The topography consists entirely of slip-off surfaces and abandoned meander cutoff loops. We note that although the channel sinuosity in this case has developed for a total dimensionless time of $t^* = 505$ including the initialization phase, the topography is only altered over the nondimensional simulation time of $t^* = 5$.

By definition, no data fall below $\Delta t_{terrace,50}/t_{vert} = 1$ (Figure 4a) because t_{vert} represents the minimum time interval between terrace levels. For all values of E_V^* with defined $\Delta t_{terrace,50}/t_{vert}$, $\Delta t_{terrace,50}/t_{vert}$ is near unity for relatively low t^*, which corresponds to limited lateral channel migration. Because reworking of existing surfaces is limited in these cases, the time interval between unique terrace levels is set only by the timescale for sufficient relief generation, and so $\Delta t_{terrace,50} \approx t_{vert}$. As t^* increases, $\Delta t_{terrace,50}/t_{vert}$ increases approximately

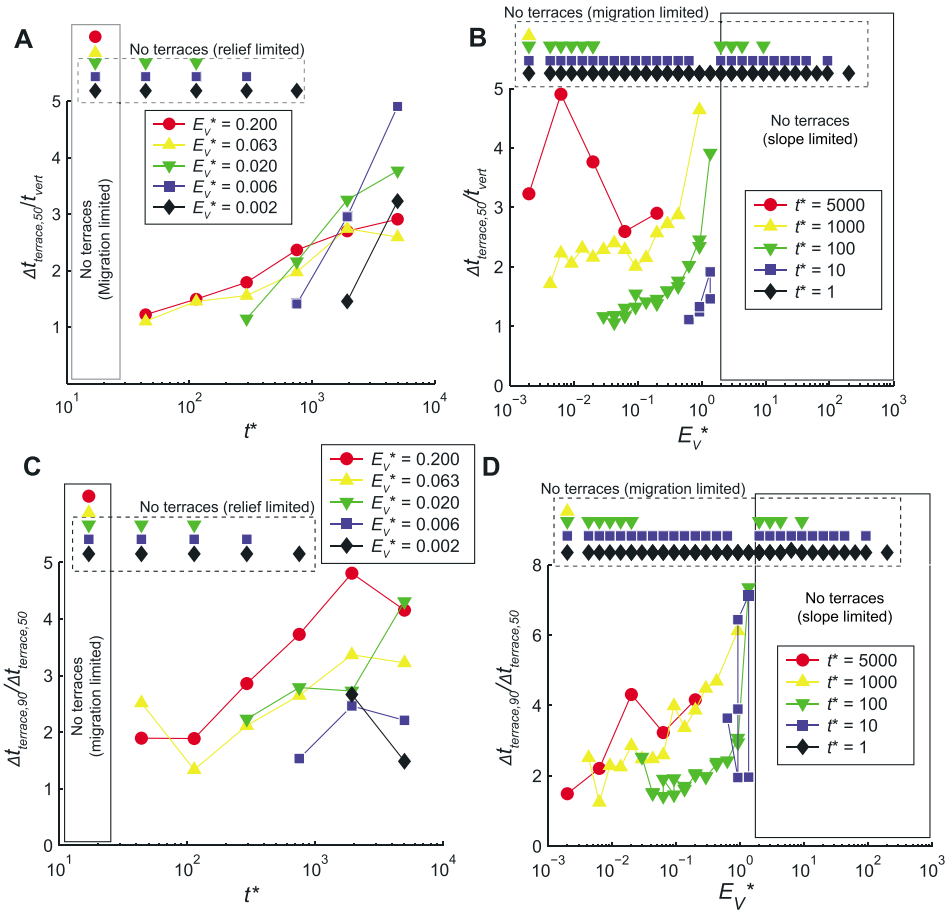

Figure 4. Dimensionless time interval between unique terrace levels ($\Delta t_{terrace,50}/t_{vert}$) for cases with constant bank strength, as a function of dimensionless simulation time (t^*) and dimensionless vertical incision rate (E_V^*). For model run sets in which one or fewer terraces typically form, $\Delta t_{terrace}$ is undefined and these cases are labeled "no terraces." Terraces may not form due to insufficient lateral channel migration (migration limited), insufficient vertical incision to generate relief for forming terraces (relief limited), because surface slopes formed by channel migration and vertical incision are too high for classification as terrace treads (slope limited) or a combination of these factors. (a) $\Delta t_{terrace,50}/t_{vert}$ versus t^* for a subset of model runs for fixed values of E_V^*. (b) $\Delta t_{terrace,50}/t_{vert}$ versus E_V^* for fixed values of t^*. (c) Ratio of the 90th and 50th percentiles of $\Delta t_{terrace}$ versus t^* for fixed values of E_V^*. (d) E_V^* for fixed values of t^*.

logarithmically because continued channel migration reworks areas previously visited by the channel. Frequent reworking of surfaces near the channel can prevent abandonment of these areas as terraces (e.g., Figure 3a) or alternatively destroy existing terraces; both processes result in longer time intervals between unique terrace levels. The logarithmic increase in $\Delta t_{terrace,50}/t_{vert}$ with dimensionless simulation time is consistent with the finding that meander belt width increases logarithmically with simulation time [*Howard*, 1996]. The margins of the meander belt are less likely to be visited by the migrating channel than areas close to the channel [*Bradley and Tucker*, 2013], so areas near the channel are preferentially reworked and terraces are less likely to be preserved there. Similarly, as the meander belt widens, the likelihood of the channel eroding past the margins of the alluvial belt decreases and the widening rate of the alluvial belt decreases. The rate of increase of $\Delta t_{terrace,50}/t_{vert}$ with increasing t^* is generally more pronounced for relatively low E_V^* because the channel is more likely to rework previously visited areas before they can be abandoned as terraces.

Figure 4b shows the time interval between unique terrace levels ($\Delta t_{terrace,50}/t_{vert}$) as a function of E_V^* for several fixed values of t^*. $\Delta t_{terrace,50}/t_{vert}$ is undefined across a broad range of E_V^* for $t^* \leq 10$ because of limited lateral channel migration in those cases. For $t^* = 100$ and $t^* = 1000$, $\Delta t_{terrace,50}/t_{vert}$ begins at a relatively low value (<2) but increases sharply as E_V^* approaches unity until $\Delta t_{terrace,50}/t_{vert}$ is undefined. This behavior occurs

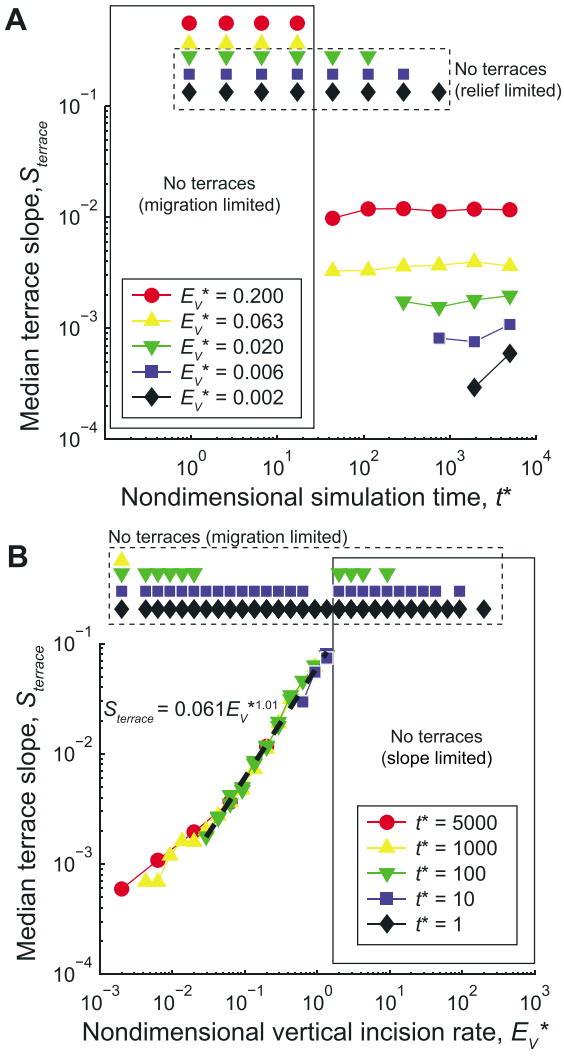

Figure 5. Median terrace slope ($S_{terrace}$) versus (a) dimensionless simulation time (t^*) for fixed values of dimensionless vertical incision rate (E_V^*) and (b) E_V^* for fixed values of t^*.

because the high relative rate of vertical-to-lateral erosion causes high surface slopes in areas eroded by the channel and results in a greater proportion of slip-off slopes relative to terraces (Figure 3c). As the number of terraces decreases, $\Delta t_{terrace,50}/t_{vert}$ increases until there are so few terraces that $\Delta t_{terrace,50}/t_{vert}$ is undefined. The transition from forming terraces to forming slip-off surfaces is sharpest near $E_V^* = 1$, where the vertical incision rate typically approaches the maximum lateral erosion rate. For $t^* = 5000$, $\Delta t_{terrace,50}/t_{vert}$ varies widely with E_V^* and is greater than for other values of t^* because of increased reworking of previously visited areas. For the high nondimensional simulation time ($t^* = 5000$) and low values of dimensionless vertical incision rate ($E_V^* < 10^{-1}$), few terraces form (due to low vertical incision rates) and terrace preservation is limited (due to extensive channel migration). Thus, the total number of terraces is relatively small and more sensitive to surface reworking than for the curves with less channel migration (i.e., lower values of t^*), which results in a higher variability in the time between terrace levels.

Figure 4c shows the distribution of time intervals between terrace levels, expressed as the ratio of the 90th and 50th percentiles of the time between unique terrace levels, as a function of t^* for several fixed values of E_V^*. For all values of $E_V^* > 0.002$, $\Delta t_{terrace,90}/\Delta t_{terrace,50}$, where it is defined, is relatively small (i.e., <3) for lower values of t^* and typically increases with t^*. The small value of $\Delta t_{terrace,90}/\Delta t_{terrace,50}$ shows that autogenic terraces do have a characteristic reoccurrence time. The increase in the variance of the time intervals between unique terrace levels with increasing t^* indicates that terraces are destroyed by increased lateral channel migration. The rate of increase of $\Delta t_{terrace,90}/\Delta t_{terrace,50}$ with t^* is similar for different values of E_V^* for $t^* < 1000$, but as in Figure 4a each curve is offset because model runs with lower E_V^* require larger t^* to generate terraces and for $\Delta t_{terrace}$ to be defined.

Figure 4d shows the variety in $\Delta t_{terrace,90}/\Delta t_{terrace,50}$ as a function of E_V^* and for several unique values of t^*. The trends in $\Delta t_{terrace,90}/\Delta t_{terrace,50}$ are similar to those in $\Delta t_{terrace,50}/\Delta t_{vert}$ (Figure 4b). Except for the model runs with $t^* = 5000$, for which terrace destruction causes large variations in the terrace age distribution, $\Delta t_{terrace,90}/\Delta t_{terrace,50}$ is relatively consistent and low until it approaches $E_V^* = 1$. Terrace formation is rarer for $E_V^* = 1$ and preferentially occurs on the insides of relatively rapidly migrating meander bends; elsewhere, slip-off surfaces form. In this case, the lower terrace formation frequency and the terrace association with exceptionally active meander bends may contribute to greater variety in $\Delta t_{terrace,90}/\Delta t_{terrace,50}$.

4.1.2. Terrace Slope

Figure 5a shows model results for median terrace slope as a function of t^* for several fixed values of E_V^*. Terrace slope is generally insensitive to t^*, except for $t^* > 1000$ and $E_V^* < 0.02$ which results in steeper terrace slopes for larger t^*. This increase in terrace slope for $t^* > 1000$ and $E_V^* < 0.02$ occurs because the terraces

formed under those conditions are broad, compound surfaces formed by the sweeping of many meander bends (Figure 3a). Consequently, some terrace surface slopes are not set instantaneously during bend migration but instead by wandering of the channel belt axis during vertical incision. For relatively high vertical incision rates, this wandering would leave a terrace (i.e., Figure 2d), but for relatively low vertical incision rates, the scarp formed at the channel cutbank is often too short and is not identified as a terrace riser (section 3.2).

Figure 5b shows median terrace slope as a function of E_V^* for several fixed values of t^*. For cases in which terraces form, there is a linear relationship between median terrace slope and E_V^* for $t^* \leq 100$. The strong collapse in the data occurs because these cases have little channel belt wandering so that the surface slope reflects the instantaneous vertical incision rate and lateral erosion rate of the channel. For $t^* > 100$ and $E_V^* < 0.1$, channel belt wandering commonly develops terraces from a composite of surfaces active at different times as the channel incises vertically; therefore, terrace slopes are slightly higher than expected solely based on the instantaneous, imposed vertical and lateral erosion rates. These results suggest that despite the kinematic complexity of meandering, terrace slope is a reliable indicator of the relative rates of vertical-to-lateral erosion, at least in cases with constant bank strength. Accounting for the influences of channel dimensions (w_c and h_c) on E_V^* (equation (1b)), the fit for $t^* \leq 100$ implies equivalence between terrace slope and the ratio of vertical incision to maximum lateral erosion rate.

4.1.3. Terrace Dip Direction

Figure 6a shows an example of the distribution of terrace dip directions for a set of model runs with fixed parameters but different initial channel planform geometries. Terrace dip direction is measured as the counterclockwise angle with respect to the mean, downstream-oriented valley axis. Terraces with $\varnothing_{terrace} = 0°$ dip parallel to the mean down-valley direction. Similarly, $\varnothing_{terrace} = \pm 180°$ corresponds to terrace dip in the up-valley direction. In this example, terrace dips are preferentially oriented perpendicular to the valley axis (i.e., ±90°). As with terrace slope, terrace dip direction may either develop through the migration of a single bend (Figure 3b) or reflect the orientation of a composite surface formed by the migration of different meander bends (Figure 3a).

Figure 6b shows the most common dip direction as a function of t^* for fixed values of E_V^*. For all values of E_V^*, terraces dip in approximately the valley-parallel directions (0° and ±180°) for $t^* < 100$ and then approach valley-perpendicular dip directions for $t^* \geq 1000$ (except for $E_V^* = 0.2$, $t^* = 5000$). Figure 6c shows the strength of the preferred terrace dip direction, expressed as the ratio of the probability for the most probable dip direction divided by the probability for the median dip direction (P_{max}/P_{median}). The strength of the preferred terrace dip direction is highest for $t^* \leq 100$ and $t^* \geq 1000$; between these values of t^*, P_{max}/P_{median} is near unity and terraces do not show a preferred dip direction. Figure 6d shows the most common dip direction ($\varnothing_{terrace}$) as a function of E_V^* for fixed values of t^*. Dip direction does not respond systematically to E_V^* but is most closely oriented in the valley-perpendicular direction for $t^* \geq 1000$. The strength of the preferred terrace dip direction does not show a consistent relationship with E_V^* (Figure 6e). The association of terraces that dip in the valley-perpendicular direction with large values of t^* (i.e., ≥1000) indicates that these surfaces form as a consequence of channel belt wandering rather than meander bend growth because multiple generations of meander bend growth and cutoff occur by $t^* = 1000$. The resulting composite surfaces dip toward the center of the valley.

4.1.4. Terrace Length

Figure 7 shows maximum terrace length normalized by channel width as a function of t^* for several fixed values of E_V^*. With some exceptions, maximum terrace length generally increases with t^*, because in time smaller terraces are preferentially destroyed by reworking (Figure 7a). The maximum terrace length is set by the domain length and is reached for cases that generate terraces with $E_V^* < 0.2$ and $t^* > 100$. Model runs that vary E_V^* for several fixed values of t^* (Figure 7b) indicate that for sufficiently long simulations, maximum terrace length plateaus at the domain length for $E_V^* \leq 10^{-1}$. These long terraces form because of the low relative rate of vertical-to-lateral erosion, and multiple generations of meander bends at different locations along the river erode a composite surface of roughly consistent elevation (Figure 3a). There is a sharp decrease in maximum terrace length for $0.1 < E_V^* < 1$ because increasing vertical incision rates cause successive generations of meander bends to erode surfaces with larger differences in elevation. This variety in surface elevations prevents the

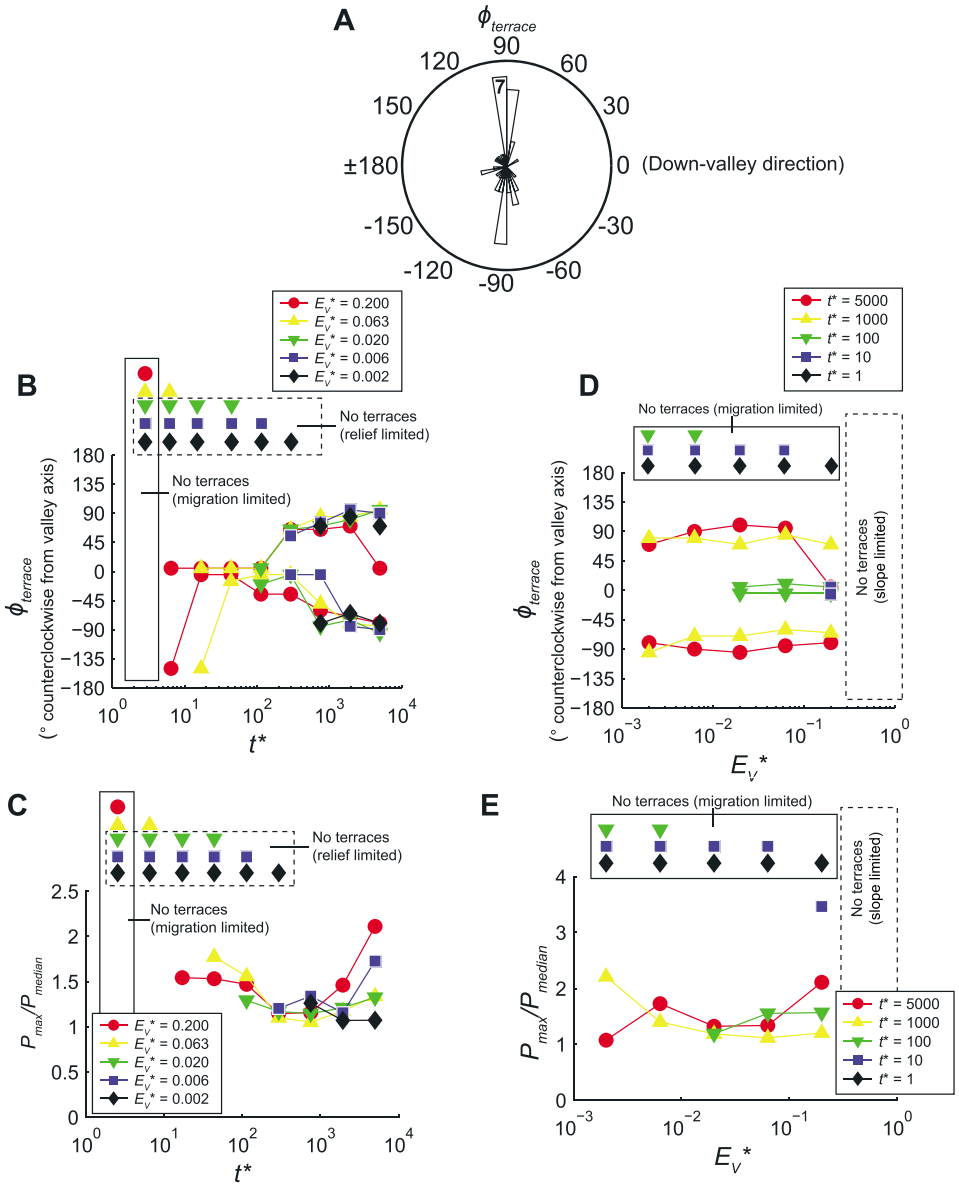

Figure 6. Terrace dip direction in model runs ($ø_{terrace}$; measured in degrees counterclockwise from the downstream-oriented, mean valley axis), as a function of dimensionless simulation time (t^*) and dimensionless vertical incision rate (E_V^*). (a) Rose diagram of $ø_{terrace}$ for $E_V^* = 0.002$ and $t^* = 5000$, combining results from 10 model runs with different initial channel planform geometries. The maximum bin count is labeled. (b) Most probable terrace dip direction versus t^* for fixed values of E_V^*. (c) The strength of the preferred terrace dip direction, expressed as the ratio of the probability for the most probable dip direction divided by the probability for the median dip direction (P_{max}/P_{median}) versus t^* for fixed values of E_V^*. (d) Most probable terrace dip direction versus E_V^* for fixed values of t^*. (e) The strength of the preferred terrace dip direction versus E_V^* for fixed values of t^*. In Figures 6b and 6d, positive and negative values of $ø$ indicate dip direction toward different sides of the valley axis and are plotted separately.

formation of longitudinally extensive, low-relief surfaces. Instead, the channel-swept areas are classified as separate and increasingly smaller terraces (Figure 3b).

4.1.5. Terrace Pairing

Paired terraces commonly occur in our model runs. Though the terraces in each pair typically form at distinct times, their differences in mean elevation are less than the threshold for classification as paired (i.e., 2 m). Paired terraces can have either of two geometries. In the first case low relative rates of vertical-to-lateral

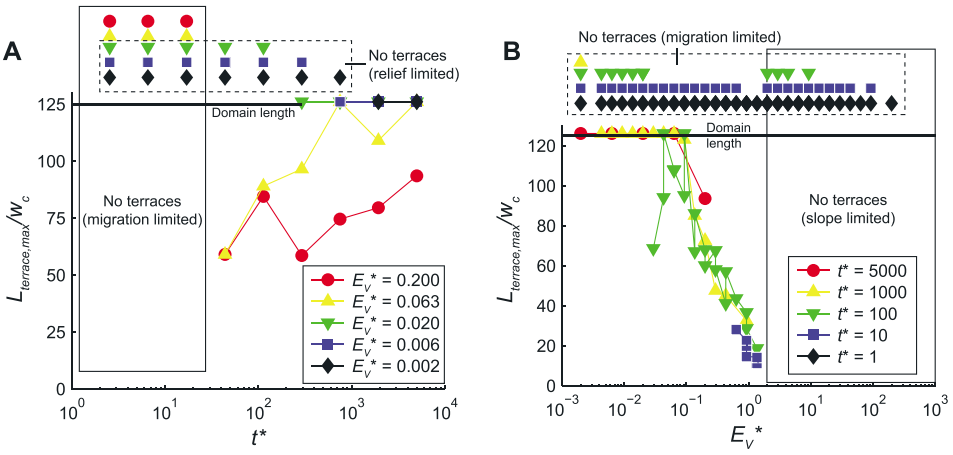

Figure 7. Maximum terrace length normalized by channel width ($L_{terrace,max}/w_c$) versus (a) dimensionless simulation time (t*) for fixed values of dimensionless vertical incision rate (E_V*) and (b) E_V* for fixed values of t*.

erosion cause the channel to wander extensively while generating little relief, which creates broad surfaces on either side of the channel (Figure 3a). In the second case, higher vertical incision rates generate relief sufficient to create a terrace during the growth and cutoff of an individual meander bend, and so numerous terraces circumscribed by meander cutoff loops form on either side of the active channel (Figure 3b).

Figure 8a shows the fraction of paired terraces (f_{paired}) as a function of t* for several fixed values of E_V*. In all cases where terraces form, f_{paired} exceeds 0.8 at the lowest values of t* and declines toward 0 as t* increases. In only one case (for E_V* = 0.006), f_{paired} increases again after its initial decrease. For model runs that vary E_V* for several fixed values of t* (Figure 8b), f_{paired} initially increases with increasing E_V* for $t^* \geq 100$ because increasing relief is generated to accommodate terraces (e.g., Figure 3). The fraction of paired terraces then decreases as E_V* approaches 1 because relatively high vertical incision rates cause high surface slopes that exceed the threshold for local relief in the terrace detection algorithm (Figure 3c and Table 2), and terraces that do form are more likely to be offset in elevation due to the high rates of relief generation.

4.1.6. Summary of Model Runs With Constant Bank Strength

For all other factors equal, model runs with low ratios of vertical-to-lateral erosion rate tend to produce longer terraces formed by the compound sweeping of several meander bends (Figures 3a and 7b). These terraces

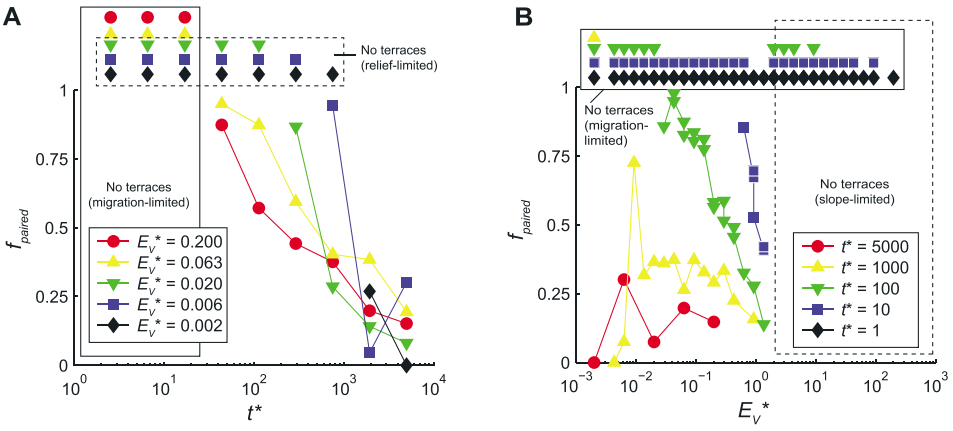

Figure 8. Fraction of paired terraces in the model domain, weighted by area (f_{paired}), versus (a) dimensionless simulation time (t*) for fixed values of dimensionless vertical incision rate (E_V*) and (b) E_V* for fixed values of t*.

dip toward the valley center (Figure 6d) with slopes higher than the ratio of vertical-to-lateral erosion rate (Figure 5b) and have terrace recurrence ages that are relatively large (Figure 4b). In contrast, terraces in model runs with high ratios of vertical-to-lateral erosion rate are commonly smaller and bounded by meander cutoff loops, as long as surface slopes are low enough to form terraces (Figures 3b and 7b). These terraces have no particular slope orientation, their gradients are directly proportional to the ratio of vertical-to-lateral erosion rate (Figure 5b), and they form frequently with a recurrence timescale that is set by the time needed to generate the relief of one terrace (Figure 4b). Pairing is maximized for moderate ratios of vertical-to-lateral erosion rate (Figure 8b). In time, lateral erosion destroys terraces resulting in larger time gaps between terraces (Figure 4a) and decreased pairing (Figure 8a). Terraces may not form for short simulation times due to insufficient vertical or lateral erosion, and slip-off surfaces rather than terraces form at very high relative rates of vertical-to-lateral erosion (Figures 3c and 4b).

4.2. Effects of Variable Bank Strength on Model Results

In this section we consider factors that control strath terrace formation and geometry for cases in which the channel encounters mixed bedrock and alluvial bank materials. For this subset of model runs, we set the dimensionless initial alluvial belt width (w_{ab}*) to 0.1, which corresponds to a zone of sediment fill one channel depth in thickness and one tenth the width of the unconfined meander belt [*Camporeale et al*., 2005] (Figure 9a). Because of the differences in bank strength between bedrock and sediment, the nondimensional vertical incision rate takes two different forms for these model runs that each reflect the lateral erosion rate in one of the bank materials (equations (2a) and (2b)). Here we vary the nondimensional vertical incision rate for bedrock banks (E_{Vb}*) from 0.004 to 4 and hold the nondimensional vertical incision rate for sediment banks constant (E_{Vs}* = 0.002). Because E_{Vs}* is fixed, the relative bank erodibility of bedrock versus sediment decreases as E_{Vb}* increases. Nondimensional simulation time is fixed to the maximum value explored in the cases with constant bank strength (t* = 5000).

Figure 9 shows examples of terrace formation for three cases with t* equal to that in Figure 3a; E_{Vb}* is between the values of E_V* in Figures 3a and 3b. Initially, the channel develops sinuosity within the sediment-filled zone but turns at sharp angles where it meets the confining bedrock walls at the margin of the alluvial belt (Figure 9a). From this initial condition, three different regimes of channel lateral migration and terrace evolution can occur [*Limaye and Lamb*, 2014]. In the first regime, the channel actively erodes the bedrock boundaries at the edge of the alluvial belt, and strath terraces form beyond the margin of the initial alluvial belt regardless of whether the channel entrenches in bedrock (Figure 9b and Movie S3 in the supporting information; E_{Vb}* = 0.02). In the second regime, the channel initially migrates through the sediment-filled zone and bevels the sediment-bedrock interface at the channel bed but eventually entrenches in bedrock. This occurs because the channel incises vertically into bedrock at a rate faster than the sediment-bedrock interface is beveled across the valley [*Limaye and Lamb*, 2014]. The entrenched channel abandons terraces, which are usually paired (Figure 9c and Movie S4 in the supporting information; E_{Vb}* = 0.07). In the third regime, the channel remains mobile within the alluvial belt but is impeded by relatively resistant bedrock at the alluvial belt boundaries. Consequently, the channel consistently erodes the same portions of the alluvial belt while incising vertically, and terraces rarely form (Figure 9d and Movie S5 in the supporting information; E_{Vb}* = 0.71). Qualitatively, terrace geometries in cases with bedrock and sediment more strongly resemble natural river terraces because terrace boundaries are sublinear at valley margins (e.g., Figures 1a and 1b) and do not directly mirror the shorter wavelengths of individual meander loops (Figure 9).

To identify model runs in which the channel entrenches in bedrock, we track the fraction of bedrock at the cutbank measured from the channel bed up to the bankfull height. The channel is classified as entrenched in bedrock if >90% of the channel length has an all-bedrock cutbank. Figure 10 differentiates cases where the channel is entrenched or unentrenched and cases that do not generate terraces. In the following paragraphs, terrace ages and geometries for the cases with variable bank strength are compared to the results for the model runs with constant bank strength collectively. In addition, we compare the results to a single case with constant bank strength and a dimensionless vertical incision rate (E_V* = 0.002) equal to the dimensionless vertical incision rate for sediment banks (E_{Vs}* = 0.002), which is indicated with a star and referred to as the control case with constant bank strength. The control case represents the distribution of terrace properties for 10 replicate simulations (section 3.3).

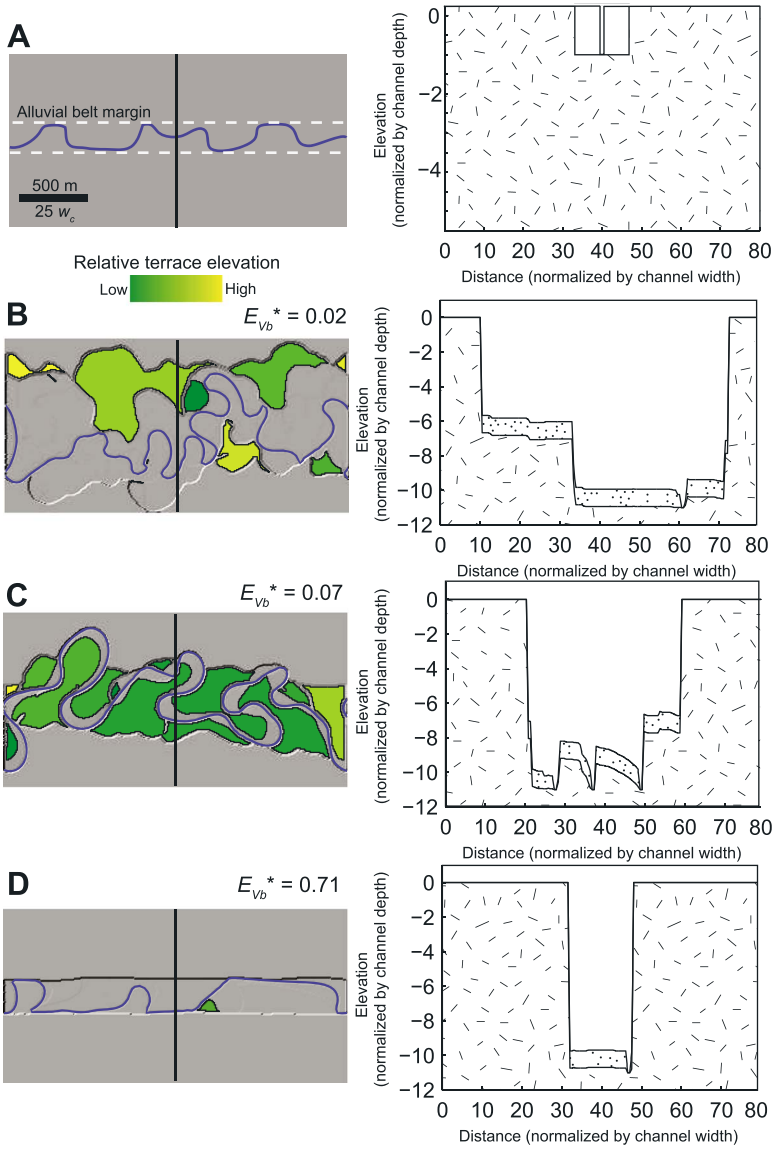

Figure 9. Types of terraces produced by the model for cases with variable bank strength. The mean flow direction in all panels is from left to right, the channel is blue, and the black lines indicate cross-section locations oriented from top to bottom across each model domain. Terraces are colored according to their mean elevation (green-yellow), and the range of mean terrace elevations is noted below. (a) The initial cross section and plan view geometry of the channel and alluvial belt, in schematic form. Because $w_{ab}^* < 1$ in this case, the initial alluvial belt width (w_{ab}) is less than unconfined alluvial belt width (w_{uab}), and initially the channel is constrained to the alluvial belt boundaries. Within the initial alluvial belt the banks are entirely sediment (dotted) and the sediment depth equals the channel depth. Areas beyond the alluvial belt and below the elevation of the channel bed are all bedrock (hatched). (b) A model run in which the channel erodes beyond the initial alluvial belt and creates extensive terraces ($E_{Vb}^* = 0.02$). The terrace elevation range is 6.8 m. (c) A model run in which the channel entrenches in bedrock and paired terraces are abandoned, largely within the initial alluvial belt ($E_{Vb}^* = 0.07$). The terrace elevation range is 4.3 m. (d) A model run in which the channel erodes vertically while largely confined to the initial alluvial belt, resulting in minimal terrace formation ($E_{Vb}^* = 0.71$). The lone terrace has a mean elevation of −8.9 m relative to the initial surface.

Figure 10a shows the dimensionless time interval between unique terrace levels ($\Delta t_{terrace,50}/t_{vert}$) as a function of E_{Vb}^*. For model runs in which terraces form, $\Delta t_{terrace,50}/t_{vert}$ varies between 1 and 3 for all but one run—a similar range as for the ensemble of cases with constant bank strength (Figures 4a and 4b) but with a greater proportion of short time intervals between terraces. $\Delta t_{terrace,50}/t_{vert}$ is also typically lower than for the control case with constant bank strength. Terraces do not form for three model runs near $E_{Vb}^* = 1$ due

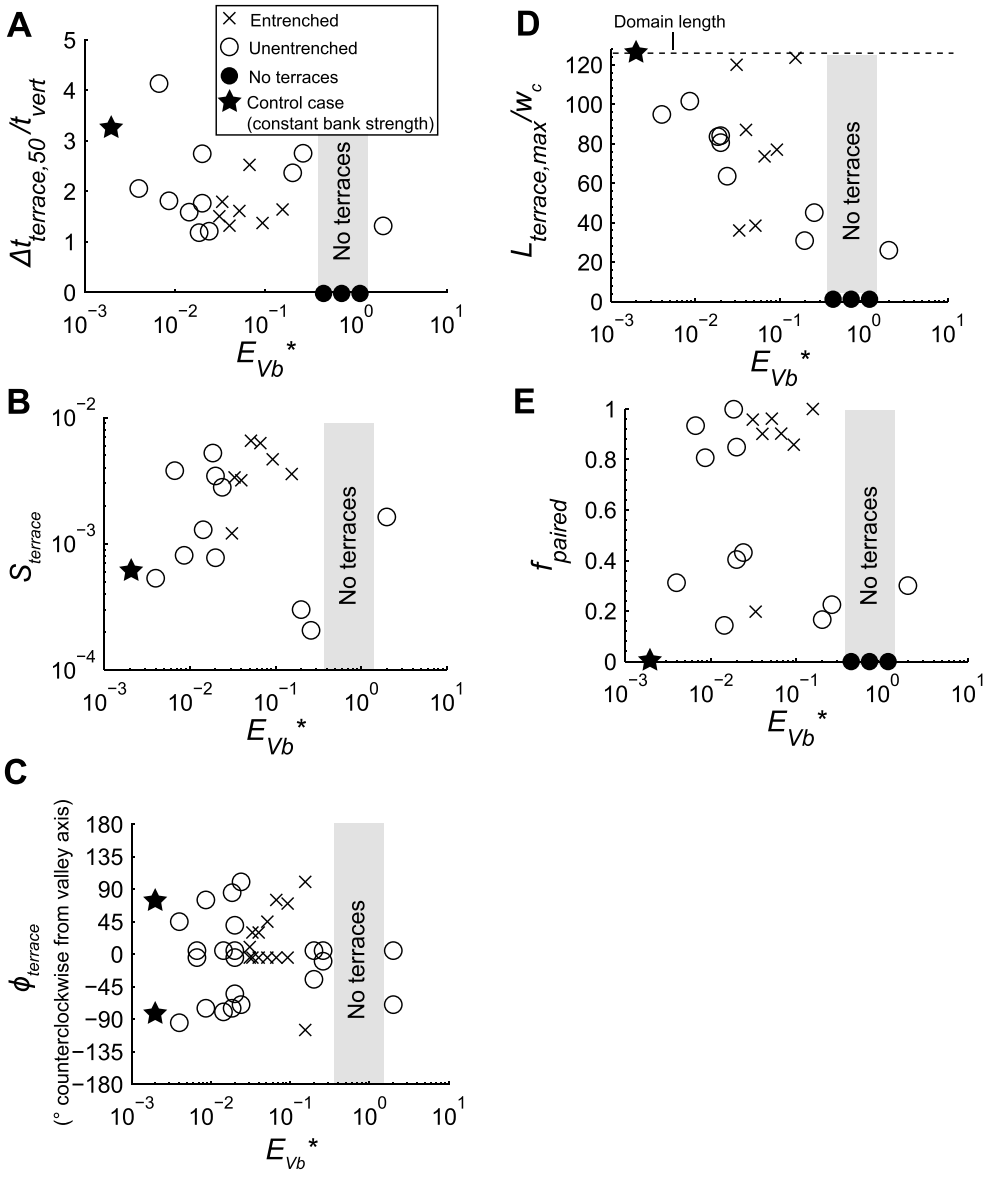

Figure 10. Time intervals between terrace levels and terrace geometry for cases with variable bank strength, as a function of nondimensional vertical incision rate for bedrock banks (E_{Vb}*). For these simulations the dimensionless simulation time ($t^* = 5000$) and dimensionless vertical incision rate for sediment banks ($E_{Vs}^* = 0.002$) are fixed, so increasing E_{Vb}* is equivalent to increasing bedrock bank strength. Model results for control cases with constant bank strength (with $t^* = 5000$ and $E_V^* = 0.002$) are indicated with black stars. (a) Median time between unique terrace levels ($\Delta t_{terrace,50}/t_{vert}$) versus E_{Vb}*. (b) Median terrace slope ($S_{terrace}$) versus E_{Vb}*. (c) Most probable terrace dip direction ($\phi_{terrace}$), measured in degrees counterclockwise from the downstream-oriented valley axis, versus E_{Vb}*. (d) Maximum terrace length (normalized by channel width) versus E_{Vb}*. (e) Fraction of paired terraces in the model domain weighted by area (f_{paired}) versus E_{Vb}*.

to highly resistant bedrock boundaries that preferentially steer meander bends to migrate down-valley and consistently sweep the alluvial belt, thus preventing terrace formation (e.g., Figure 9d). For cases in which terraces form, there are no systematic trends between $\Delta t_{terrace,50}/t_{vert}$ and E_{Vb}*.

Median terrace slope (Figure 10b) generally increases with E_{Vb}* for $E_{Vb}^* < 0.1$, similar to the trend for cases with constant bank strength (Figure 5b) but with more variability. The control case with constant bank strength yields a lower terrace slope than a majority of the cases with variable bank strength. For

$E_{Vb}^* > 0.1$, terrace slopes no longer increase. Thus, terrace slope is a less reliable indicator of the ratio of vertical-to-lateral erosion rate when bank materials are not uniform.

The preferred terrace dip direction (Figure 10c) shows no consistent relationship with E_{Vb}^*, and for several data points terraces preferentially dip valley perpendicular (i.e., ±90°). In comparison, a valley-perpendicular terrace dip direction occurs for a more continuous range of dimensionless vertical incision rate for cases with constant bank strength with $t^* \geq 1000$ (Figure 6b), including the control case with constant bank strength. Maximum terrace length (Figure 10d) approaches the domain length for $E_{Vb}^* < 10^{-2}$, similar to cases with constant bank strength (Figure 7); maximum terrace length generally declines as E_{Vb}^* increases except for two entrenched cases.

Paired terraces in the cases with variable bank strength form through two mechanisms. First, in cases with relatively erodible bedrock and thus low vertical incision rates (i.e., $E_{Vb}^* \leq 0.03$; Figure 9b), paired terraces form by channel belt wandering with low-relief generation, similar to cases with constant bank strength. Second, channel entrenchment in bedrock can abandon extensive paired terraces in the former alluvial belt (Figure 9c). For the range of E_{Vb}^* explored in the model runs, terraces do not occur simultaneously along adjacent, growing meander bends, as occurs in cases for the model runs with constant bank strength. The fraction of paired terraces (Figure 10e) does not vary systematically with E_{Vb}^*, but the highest values of f_{paired} occur for $E_{Vb}^* < 0.1$ except for cases in which the channel entrenches. Paired terraces are relatively rare for $E_{Vb}^* > 0.1$. The control case with constant bank strength does not generate paired terraces.

In summary, with significant differences in sediment and bedrock bank strength, terraces have smaller age differences, are reduced in length, and are more commonly paired. These differences are consistent with reduced lateral migration due to the presence of resistant bedrock, which in cases becomes the dominant bank material due to channel entrenchment. Bedrock banks limit the cross-valley growth of meander bends and suppress formation of extensive, compound surfaces by multiple meander sweeps. The evolving, spatial differences in bank strength can steer the channel away from areas it has already migrated across, which favors preservation of terraces formed closely in time. These unsteady migration patterns, coupled with vertical incision, cause the formation of surfaces whose slopes and dip directions are less deterministic than for cases without bank strength differences.

4.3. Effects of Pulses of Vertical Incision on Model Results

Here we present a simple example, rather than an exhaustive exploration of parameter space, to show how autogenic terraces may overprint terraces formed by pulses of vertical incision. Figure 11 shows topography formed by a meandering river over 100,000 years for three scenarios: the first with pulsed vertical incision on a repeating 25,000 year timescale, the second for a constant vertical incision rate (similar to model runs in section 4.1), and the third with pulses of vertical incision with greater amplitude but shorter duration than in the first case. The total vertical incision is the same in all cases, bank strength is constant, and the maximum lateral erosion rate (1 m/yr) corresponds to sediment bank materials. Thus, over the course of the model runs the average nondimensional vertical incision rate is the same in all three cases ($E_V^* = 0.004$, slightly greater than in Figure 3a). The nondimensional simulation time ($t^* = 5000$) is equal to that in Figures 3a and 9b–9d, and the channel width-to-depth ratio is also fixed to its baseline value ($w_c^* = 20$). The different vertical incision histories (Figures 11a–11c) cause differences in topography (Figures 11d–11f), but the lateral erosion history is the same in all three cases. Mean terrace elevations are binned at 1 m intervals (i.e., Δz; Figures 11j–11l), mean terrace formation times are binned at 5 kyr intervals (Figures 11m–11o), and the terrace area represented in each terrace formation time bin is normalized by the total terrace area (Figures 11m–11o).

Strikingly, the topography formed in the two cases with pulses of vertical incision (Figures 11a and 11c) closely resembles the topography formed in the case without pulses of vertical incision (Figure 11b). Moderate differences in the topography are evidenced by the map view extent of terraces (Figures 11d–11f) and the topographic cross sections (Figures 11g–11i). This comparison illustrates that meandering can dictate valley topography, which in this scenario is relatively insensitive to the history of vertical incision. In all three model runs the terrace area distribution is dominated by terraces formed at two or fewer time

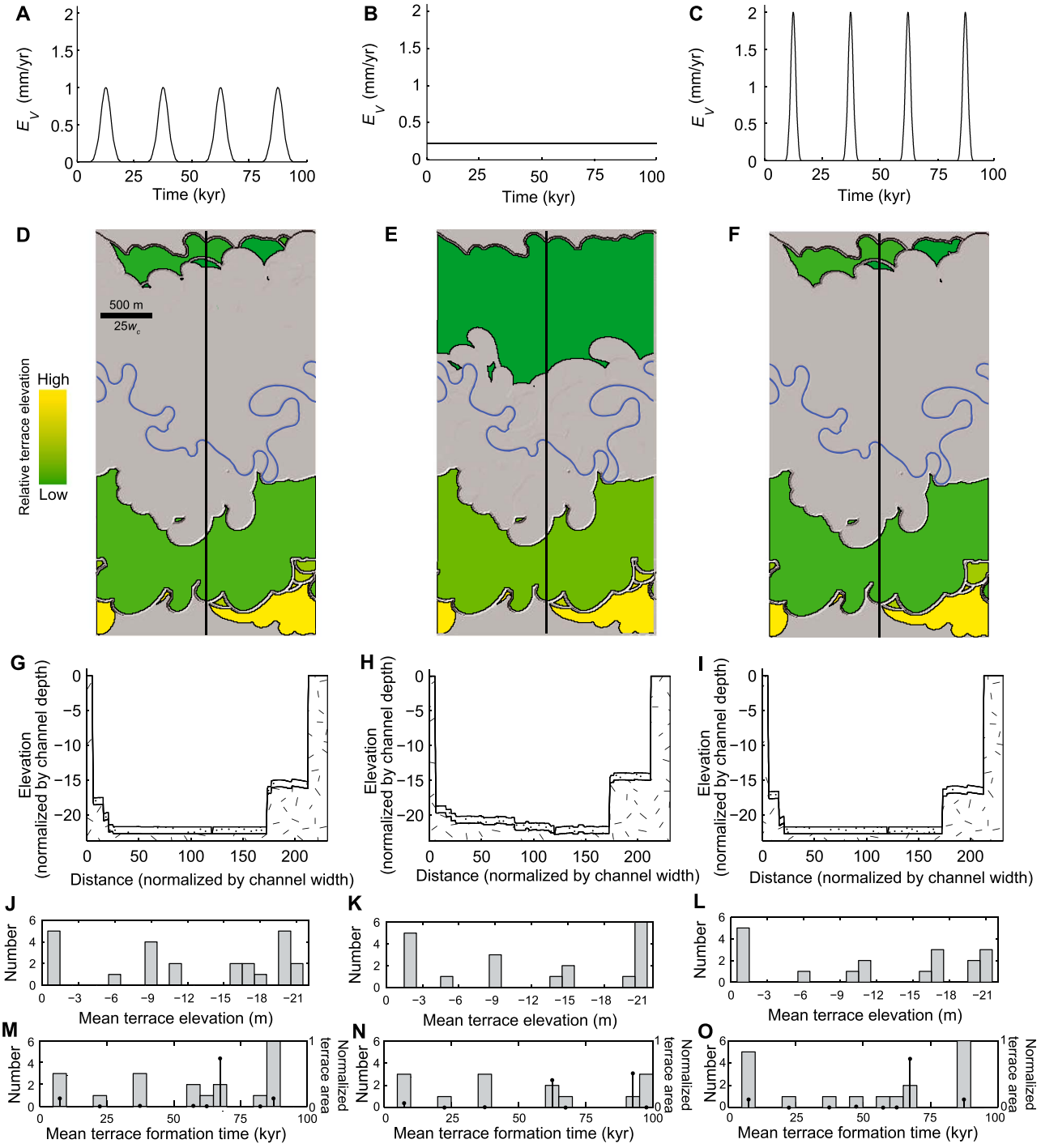

Figure 11. Examples of terrace formation by pulses of vertical incision (left and right panels) and constant vertical incision (center panels). (a–c) Vertical incision rate versus elapsed time. (d–f) Shaded relief of topography overlain by automatically detected terraces. The channel is shown in blue and the black lines indicate cross-section locations oriented from top to bottom across each model domain. Mean flow is from left to right. Total vertical incision is the same in all cases. Terraces are colored according to their mean elevation (green-yellow); elevation distributions are given in Figures 11j–11l. (g–i) Topographic cross sections indicating bedrock (hatched) and sediment (dotted). (j–l) Histograms of mean terrace elevation, binned at 1 m intervals. (m–o) Histograms of mean terrace formation time (bars and left axis), binned at 5 kyr intervals. The corresponding terrace area for each mean formation time, normalized by total terrace area, is also plotted (points and right axis).

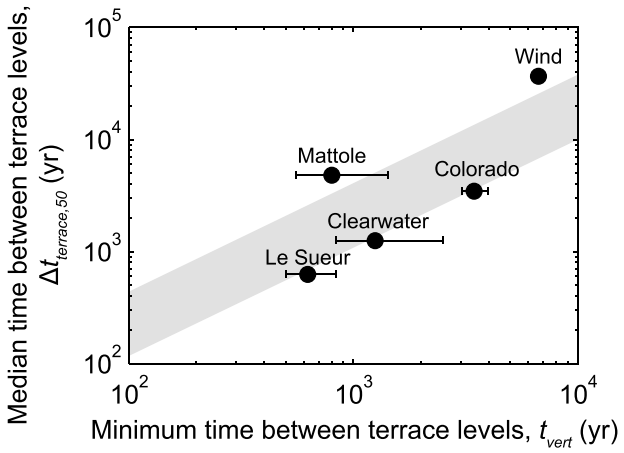

Figure 12. The estimated median time between terrace levels ($\Delta t_{terrace,50}$) versus the minimum time interval between terrace levels (t_{vert}), both assuming a constant vertical incision rate at each site. The shaded area indicates the range of time intervals between terrace levels in the simulations with constant vertical incision rates. Error bars for the Wind River are within the plotted point.

periods from the second half of the run, highlighting the preferential preservation of younger terraces (Figures 11m–11o).

The first case with pulsed vertical incision includes four full cycles of vertical incision (Figure 11a and Movie S6 in the supporting information). Yet several more unique terraces levels form (Figure 11j) with different ages (Figure 11m) because the pulses are not instantaneous, and lateral channel migration during periods of relatively high rates of vertical incision can create more than one terrace level. In comparison, the case with a constant vertical incision rate yields a greater plan view terrace extent (Figure 11e and Movie S7 in the supporting information) and also forms several terraces at distinct levels (Figure 11k) and times (Figure 11n). From section 4.1, the timescale for terrace formation ($\Delta t_{terrace,50}$) for a constant vertical incision rate is approximately 1 to 4 times the minimum time interval between terrace levels (t_{vert}; equation (9)). For the model run in Figure 11e, this corresponds to $\Delta t_{terrace,50} \approx 5000$ to 20,000 years, which approaches the 25,000 year period of vertical incision pulses. Thus, in this example the intrinsic frequency of terrace generation by meandering is similar to the frequency of terrace formation driven by external forcing.

The model run with relatively brief, high-amplitude pulses of vertical incision (Figure 11c) might be expected to produce a set of terraces with stronger distinctions in terrace elevation and terrace formation time compared to the case with more gradual vertical incision pulses (Figure 11a). Instead, the mean terrace elevations (Figure 11l) and surface formation times (Figure 11o) in the case with sharp vertical incision pulses are similar to those in the case with more gradual pulses (Figures 11j and 11m, respectively). Notably, as in the case with gradual incision pulses, the case with sharper incision pulses does not yield a direct correspondence between the number of pulses (Figure 11c) and the number of unique terrace formation times (Figure 11o). As with the larger-scale valley topography, terrace properties are strongly influenced by meandering and relatively insensitive to vertical incision history.

5. Comparison of Model Results to Natural River Valleys

In the following sections we analyze terrace geometry for the valleys introduced in section 2.2 and compare terrace geometry to the model results. We focus the comparison on the results in section 4.1 for model runs with constant bank strength and steady vertical incision rates for simplicity. We also make comparisons for a fixed dimensionless simulation time, $t^* = 5000$. This exercise is not meant to assert that the field cases owe their terraces to the mechanics in our model. Indeed, far more detailed field research, dating, and sedimentology have been devoted to these case studies than what we present here [*Blum and Valastro*, 1994; *Merritts et al*., 1994; *Hancock et al*., 1999; *Wegmann and Pazzaglia*, 2002; *Wolkowinsky and Granger*, 2004; *Gran et al*., 2013]. Rather, our goals are to illustrate that autogenic terraces generated by the simplest version of our model (steady vertical incision with constant bank strength) can produce terraces with realistic geometries, slopes, extents, pairing fractions, and age differences. Furthermore, the properties of the autogenic terraces in our model overlap in cases with expectations for terrace formation induced by climate change (as in Figure 11), suggesting that the two mechanisms are likely overprinted for some natural cases. Only the Mattole River strath terraces are thought to have formed by meandering and steady vertical incision [*Merritts et al*., 1994], with the terraces from the other sites attributed to pulses of vertical incision from various mechanisms. In section 6 we discuss a possible strategy for separating autogenic terraces from those formed by other mechanisms.

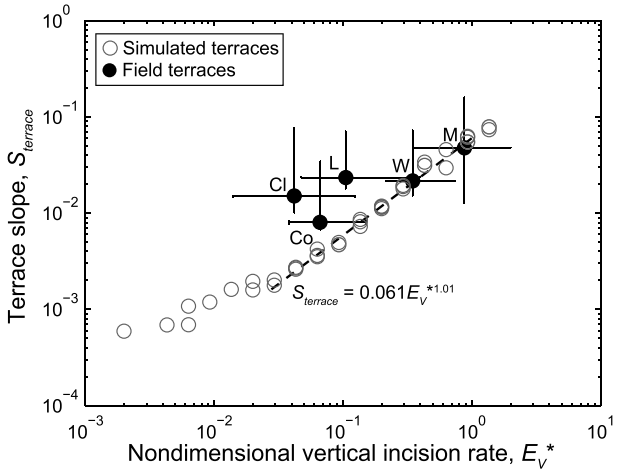

Figure 13. Terrace slope ($S_{terrace}$) for natural river valleys versus estimated dimensionless vertical incision rate (E_V^*). Labels indicate terraces for the Colorado (Co), Le Sueur (L), Clearwater (Cl), Wind (W), and Mattole Rivers (M). Error bars indicate the 90th and 10th percentiles of slope for different terraces in each river valley. The regression corresponds to the simulated terraces.

Besides the possibility of different terrace formation mechanisms, the natural terraces differ from those in our model runs in other ways. Our model assumes that a blanket of sediment with uniform thickness covers strath surfaces, such that terrace surface geometry reflects strath geometry. The same assumption may not hold for field cases [*Fuller et al.*, 2009]. Terrace dip direction and slope magnitude for field cases may be altered by hillslope processes, including colluvium accumulation near terrace margins [*Niviere and Marquis*, 2000] and terrace dissection [*Wegmann and Pazzaglia*, 2009]. Terrace slope can reflect a complicated history of channel gradients and knickpoint propagation [*Frankel et al.*, 2007; *Finnegan*, 2013], which are not included in our model runs. Moreover, as explained in section 3.2.2, for all field examples the terrace elevations are measured with respect to the local active channel bed elevation, which effectively removes channel bed gradient from the terrace data. While this provides a more robust comparison to our simulations with zero bed slope, it masks down-valley tilts of the field terraces, especially for some of the higher gradient rivers we analyzed. Despite these complications, results show similarities between our modeled autogenic terraces and some of the field examples.

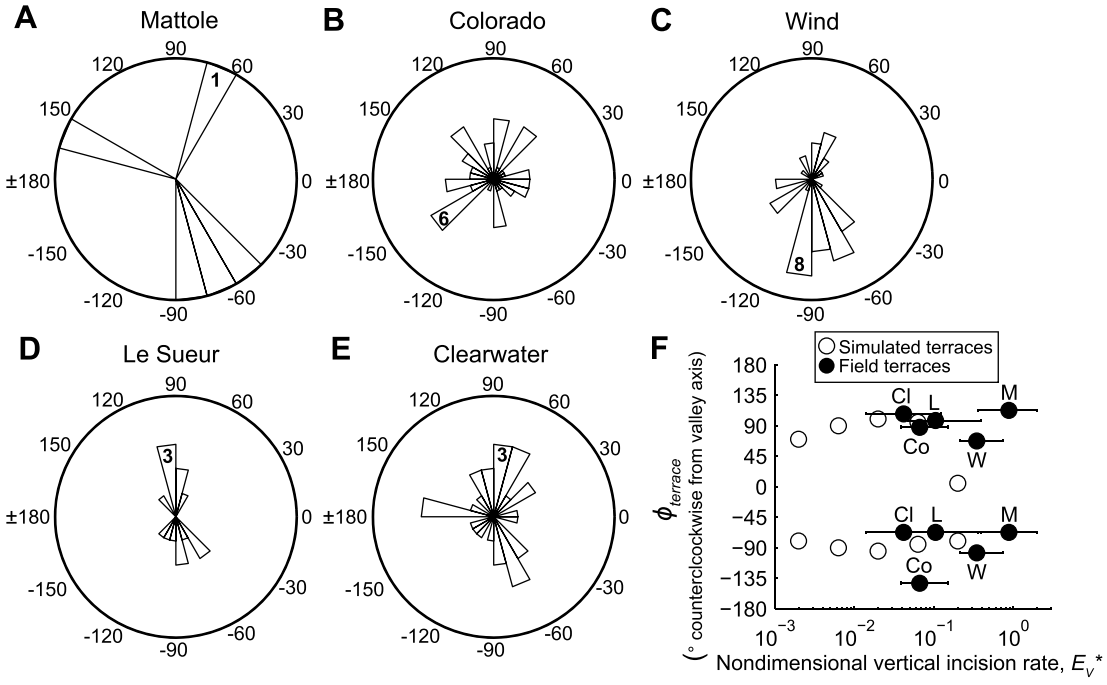

Figure 14. (a–e) Rose diagrams of terrace dip direction ($ø_{terrace}$) for natural valleys. $ø_{terrace}$ is measured counterclockwise with respect to the downstream-oriented valley axis. The maximum bin count is labeled. (f) $ø_{terrace}$ versus nondimensional vertical incision rate (E_V^*). Positive and negative values, indicating dip direction toward different sides of the valley axis, are plotted separately. Valley labels correspond to those in Figure 13. Dip direction is averaged in cases where multiple direction bins have the same count.

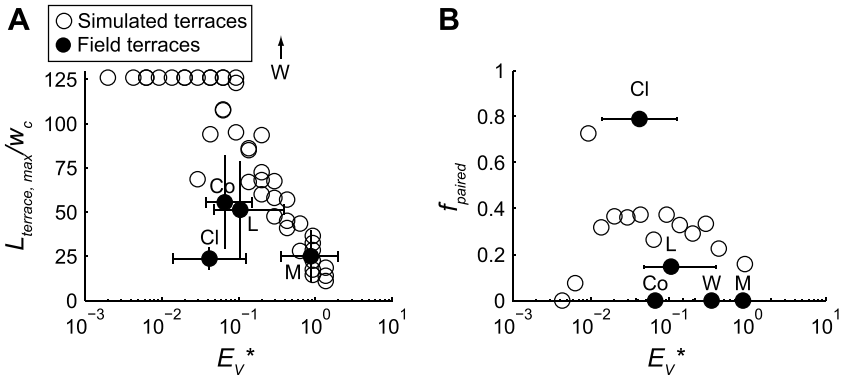

Figure 15. (a) Maximum terrace length normalized by channel width ($L_{terrace,max}/w_c$) versus estimated dimensionless vertical incision rate (E_V*) for natural and simulated river valleys. Terraces with $L_{terrace}/w_c = 125$ are as long as the model domain. Error bars indicate the upper and lower bounds on terrace length; filled symbols are plotted using the mean of these bounds. The arrow indicates that the Wind River terraces have a range $L_{terrace,max}/w_c$ that is off scale (150–450). (b) Fraction of paired terraces, weighted by terrace area, versus estimated E_V* for natural and simulated river valleys. Labels in both panels correspond to those in Figure 13.

5.1. Time Interval Between Terrace Levels

Figure 12 shows the estimated, median time between terrace levels versus the minimum time interval between terrace levels for each valley. Compared to the model runs with constant vertical incision rates, the estimated time between terrace levels is slightly longer for the Wind River; slightly longer but within the t_{vert} error estimates for the Mattole River; and slightly shorter but within the t_{vert} error estimates for the Le Sueur, Clearwater, and Colorado Rivers.

5.2. Terrace Slope

The natural terrace slopes are similar to the simulated terrace slopes for the Wind and Mattole Rivers (Figure 13). Terrace slopes are higher but within error estimates for nondimensional vertical incision rate (E_V*) for the Colorado and Le Sueur Rivers, and terrace slopes for the Clearwater River are substantially higher than predicted with the model. We speculate that dissection of terrace treads or errors in mapping (i.e., inclusion of relatively steep areas at terrace margins) may contribute to these relatively high slopes.

5.3. Terrace Dip Direction

Figure 14 shows the distribution of terrace dip directions ($\varnothing_{terrace}$) for each of the field sites, measured counterclockwise with respect to the downstream-oriented valley axis. The Mattole River (Figure 14a) possesses the fewest terraces; while the dip directions are varied, no terraces dip parallel to the valley, which is consistent with the conceptual model of *Merritts et al.* [1994] for terraces formed by lateral erosion and constant vertical incision. Terraces for the Colorado (Figure 14b), Wind (Figure 14c), Le Sueur (Figure 14d), and Clearwater Rivers (Figure 14e) all show a variety of orientations and preferred orientations in directions oblique or nearly perpendicular to the valley axis. The dominant terrace dip direction for each valley plotted against E_V* shows that terraces oriented nearly perpendicular to the valley trace occur at a variety of values of E_V*, which is consistent with the model predictions.

5.4. Terrace Length

In contrast to the model runs with constant bank strength, the natural terraces do not exhibit an inverse relation between E_V* and maximum terrace length normalized by channel width ($L_{terrace,max}/w_c$) (Figure 15a). Notably, the Clearwater and Mattole River terraces have similar $L_{terrace,max}/w_c$, despite their large difference in E_V* (Table 1). The exceptionally large $L_{terrace,max}/w_c$ for the Wind River greatly exceeds the modeled maximum terrace length for the same value of E_V* (for which model domain length is greater than maximum terrace length), which suggests that at least some of the Wind River terraces formed through means other

than meandering with constant vertical incision. Maximum terrace length for the Mattole River is similar to the model runs. Terraces for the Colorado and Le Sueur Rivers are somewhat smaller in length than predicted by the model but within uncertainties for E_V^* and $L_{terrace,max}/w_c$. The model does not include tributaries, which bound some terraces in the Colorado River valley and thus limit their length.

5.5. Terrace Pairing

Figure 15b shows the fraction of paired terraces, weighted by terrace area, for each of the field sites. Only the Le Sueur River and Clearwater River terraces meet the pairing criteria of (1) adjacency across the river and (2) mean terrace elevation within a threshold range (2 m). The existence of paired terraces on the Le Sueur River is consistent with models that predict paired terraces for cases with pulsed vertical incision. The Clearwater River terraces are much more paired than predicted by our model runs, whereas the absence of paired terraces for the Colorado, Wind, and Mattole Rivers differs strongly with model predictions of $f_{paired} \approx 0.15–0.40$ for those values of E_V^*.

6. Discussion

Modeling by *Finnegan and Dietrich* [2011] also involved terrace formation linked to meandering, wherein meander growth and cutoff generated knickpoints that caused unsteady vertical incision rates. In comparison, the present modeling indicates that a broader suite of meandering rivers—including low-sloping rivers without knickpoints—can generate terraces under steady external forcing after the river generates sufficient relief to abandon a terrace (i.e., $\Delta t_{terrace,50}/t_{vert} \approx 1–4$; Figure 4). Notably, *Finnegan and Dietrich* [2011] reported only unpaired terraces, but using objective criteria (section 3.2) paired terraces occur in our model because of longer dimensionless simulation times (i.e., more extensive lateral channel migration) and the use of a periodic boundary condition that allows free motion of the channel belt axis. Although these paired terraces generally form at different times, their age differences are less than or equal to t_{vert} (equation (9)), which varies from 10^2 to 10^4 years for the model parameters tested here. This range of age differences resembles uncertainties for field dating techniques (i.e., approximately 10^2 to 10^4 years, depending on terrace age [*Hancock et al*., 1999; *Wegmann and Pazzaglia*, 2002]).

Climate change has undoubtedly driven dramatic changes in water discharge and sediment supply, particularly near the headwaters of glaciated catchments [*Hallet et al*., 1996; *Hancock and Anderson*, 2002]. The magnitude of water and sediment supply variations in these catchments, however, is likely much larger than in many other locations. Nonetheless, a similar model of terrace formation driven by climate change has been adopted for many catchments that likely experience smaller changes in water and sediment supply, including in the U.S. the coast ranges of Oregon [*Personius et al*., 1993] and California [*Bull*, 1991; *Fuller et al*., 2009; *DeVecchio et al*., 2012] and the Texas Coastal Plain [*Blum and Valastro*, 1994]. While in some landscapes dramatic climate change is also indicated by moraines and other glacial features [e.g., *Hancock et al*., 1999], in settings far from the glacial headwaters, terraces are often the primary geomorphic markers used to infer climate change [e.g., *Bull*, 1991; *Personius et al*., 1993; *Blum and Valastro*, 1994; *Fuller et al*., 2009]. The model results presented herein suggest that the intrinsic unsteadiness of lateral erosion should be considered as a null hypothesis for terrace formation in many landscapes, and the frequency of terrace formation by autogenic processes and external forcing may overlap in cases (Figure 11).

Using the elevation difference between terrace levels as a proxy for time, the estimated time between unique terrace levels is consistent with terrace formation under constant vertical incision rates for some natural river valleys (Figure 12). Strath terrace ages and elevations compiled by *Finnegan et al*. [2014], however, demonstrate that for many bedrock river valleys the estimated vertical incision rate declines as the measurement timescale increases, which can be explained by hiatuses in vertical incision. Thus, for mixed bedrock-alluvial rivers the model results presented here represent an end-member vertical incision scenario that in nature is likely overprinted by vertical incision hiatuses.

Our model results indicate that as a valley evolves, the river commonly reworks areas it has visited previously and thus biases surviving terraces toward older ages (Figure 4a). This bias in preservation potential has been suggested from dated alluvial units [*Lewin and Macklin*, 2003] and from modeling of floodplain sediment age [*Bradley and Tucker*, 2013] but has only been hypothesized to occur for strath terraces [*Wegmann and Pazzaglia*, 2002]. Autogenic terrace formation and destruction by meandering may help explain the frequent

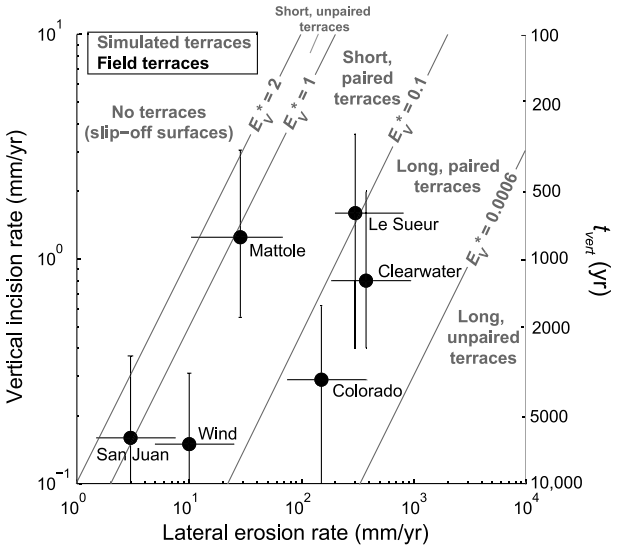

Figure 16. Summary of model predictions (gray) for terrace occurrence, pairing, and length as a function of vertical incision rate and lateral erosion rate. Black markers indicate estimated erosion rates for natural river valleys; uncertainties in vertical incision rates for the San Juan, Wind, and Colorado Rivers extend below the *x* axis limit. The minimum time interval between terrace levels (t_{vert}) is indicated on the right. The time in between terrace levels can exceed t_{vert} for relatively long simulation times and low dimensionless vertical incision rates (see Figure 4).

discordance between terrace levels and climate cycles [e.g., *Pan et al*., 2003; *Bridgland and Westaway*, 2008]. In particular, our results show that channel migration can (1) cause more terrace levels (Figure 11j) to form than vertical incision pulses (Figure 11a), (2) cause terraces to form without incision pulses (Figure 11k), and (3) destroy existing terraces (Movie S7 in the supporting information). These dynamics do not occur in terrace models such as *Hancock and Anderson* [2002] in which meandering is omitted and valley widening is only allowed in one direction.

Terraces generated by meandering rivers have been hypothesized to dip toward the valley center with a slope equal to the ratio of vertical-to-lateral erosion rate [*Merritts et al*., 1994; *Fuller et al*., 2009; *Finnegan and Dietrich*, 2011]. For our model runs with broad terraces formed by the migration of several meander bends, the terraces do tend to dip toward the valley center, but with slopes that are sometimes steeper than the ratio of channel vertical to lateral incision rates (e.g., for $t^* > 1000$ and $E_V^* < 0.01$). Although numerous factors could complicate the interpretation of erosion rates from terrace slope, the model runs here demonstrate the plausibility of the approach.

Paired terraces are often thought to be diagnostic of pulses of vertical incision [e.g., *Merritts et al*., 1994; *Wegmann and Pazzaglia*, 2002], but they also commonly form in our model runs with both constant bank strength (Figure 8) and variable bank strength (Figure 10d). In some cases the model runs produce paired terraces that are more abundant than observed for the Le Sueur River (Figure 15b). Notably, terraces commonly mapped as paired in the Colorado, Wind, and Mattole River valleys are sufficiently offset in mean elevation that the objective algorithm used here classifies them as unpaired. Thus, the threshold elevation difference used to classify terraces as paired or unpaired may weigh heavily on interpretation. Considering that pairing may also decrease in time due to terrace destruction (Figure 8a), pairing does not appear to be a reliable indicator of terrace formation process in valleys where channel migration is extensive. Terrace length appears to be a more robust indicator of formation process, as especially long terraces (i.e., $L_{terrace,max}/w_c > 100$) only form by meandering with constant vertical incision for $E_V^* < 0.1$ (Figure 7b). Thus, based on the model, the existence of long terraces (i.e., $L_{terrace,max}/w_c > 100$), combined with $E_V^* > 0.1$, rules out terrace formation by meandering with constant vertical incision, which is the case for the longest Wind River terraces (Figure 15a).

The unsteadiness of lateral erosion by meandering is amplified by the presence of mixed bedrock and alluvial banks that cause spatial and temporal transitions between conditions of high channel mobility in sediment banks and low mobility in bedrock banks [*Lewin and Brindle*, 1977; *Limaye and Lamb*, 2014]. This behavior can generate relatively straight terrace margins (Figure 9), as commonly occur for natural river terraces where they meet adjoining hillslopes (Figures 1a and 1b). The heightened unsteadiness of channel migration with spatial differences in bank strength indicates that the terrace record for these cases may be particularly susceptible to autogenic alteration. In comparison to the cases with constant bank strength, the larger scatter in terrace properties for the cases with variable bank strength (Figure 10) may result, in part, from the lack of averaging over replicate model runs. Some variability in terrace properties, however, likely results from the different regimes of valley widening in the cases with variable bank strength (Figure 9) that can be highly sensitive to initial conditions [*Limaye and Lamb*, 2014].

Model results are summarized for dimensional erosion rates in Figure 16, which shows different regimes of terrace development for constant vertical incision rates: (1) no terraces; (2) short (i.e., $L_{terrace,max}/w_c < 100$), unpaired (i.e., $f_{paired} < 0.25$) terraces; (3) short (i.e., $L_{terrace,max}/w_c < 100$), paired (i.e., $f_{paired} > 0.25$) terraces; (4) long (i.e., $L_{terrace,max}/w_c > 100$), paired (i.e., $f_{paired} > 0.25$) terraces; and (5) long (i.e., $L_{terrace,max}/w_c > 100$), unpaired (i.e., $f_{paired} < 0.25$) terraces. The lack of significant terrace development in the San Juan River valley is consistent with the model prediction that any eroded surfaces are likely small terraces or slip-off surfaces due to the high relative rate of vertical-to-lateral erosion. The model further predicts that terrace geometries thought to indicate formation by climate change are more likely to develop autogenically for certain types of rivers. For example, the Colorado River valley would be expected to develop long, paired terraces autogenically due its low relative rate of vertical-to-lateral erosion. If long, paired terraces are a signature of climate change, then this signature is unlikely to be confounded by autogenic terrace formation by meandering in rivers with maximum lateral erosion rates less than 20 mm/yr, such as the Wind River.

The terrace recurrence timescale offers another criterion for distinguishing terrace formation mechanisms. The typical terrace recurrence time is between one and four times t_{vert} (Figure 4a); the latter is indicated in Figure 16. Model results indicate that short, unpaired terraces are expected to have recurrence times of less than 1000 years for vertical incision rates greater than 1 mm/yr and lateral erosion rates greater than 10 mm/yr. In contrast, recurrence times greater than 1000 years are expected for lower vertical and lateral erosion rates. Autogenic terraces that are long, paired, and occur at timescales typical of major climate change (e.g., 10,000 years) only form for vertical incision rates less than 1 mm/yr and lateral erosion rates greater than 20 mm/yr. Thus, in order to identify terraces that record climate change, the best environments are those with terraces whose ages and geometries differ strongly from those predicted for autogenic terraces.

7. Conclusions

We utilize a numerical model of river meandering with vertical incision to identify controls on the age distribution and geometry of river terraces that form with constant external forcing. Model results indicate that for a variety of constant vertical incision rates and lateral erosion rates, rivers can generate terraces due to the intrinsically unsteady patterns of lateral erosion by meandering. The ratio of channel vertical-to-lateral erosion rate and the simulation time exert the strongest controls on terrace age and geometry. The observed time interval between unique terrace levels scales with the timescale of vertical incision required to generate sufficient relief to generate a new terrace, and the observed time interval between terrace levels increases with simulation time due to reworking of previously visited areas. Terrace formation ceases for high ratios of channel vertical-to-lateral erosion rate because eroded surfaces have high surface slopes characteristic of slip-off surfaces. Model runs suggest that the autogenic terraces have several consistent properties including (1) surface slopes that are commonly proportional to the ratio of vertical-to-lateral erosion rate during terrace formation, (2) dip directions oriented perpendicular to the valley axis for low ratios of vertical-to-lateral erosion rate and long channel evolution times, (3) greater along-valley extents for low ratios of vertical-to-lateral erosion rate, and (4) a maximum in the spatial extent of paired terraces for intermediate ratios of vertical-to-lateral erosion rate. Spatial variations in bank strength between bedrock and sediment cause terrace ages to be separated by shorter time intervals. These terraces also are smaller and more frequently paired than terraces formed in cases with constant bank strength and also have sublinear terrace margins, similar to many natural river terraces.

Case examples of natural river terraces show a modest increase in terrace slope with the estimated vertical-to-lateral erosion rate ratio and commonly dip toward the valley center. Maximum terrace length is the most reliable geometric indicator of terrace formation by episodic vertical incision; for moderate to high values of dimensionless vertical incision rate, the lengths of autogenic terraces are relatively limited because successive generations of meander bends erode surfaces at different elevations. For landscapes without independent indicators of climate change, river terrace formation by intrinsic meandering processes should be considered as the null hypothesis. Long, paired terraces with millennial-scale intervals between terrace levels, which have been suggested to indicate formation driven by external factors, are likely to develop autogenically in landscapes with relatively high lateral erosion rates and moderate vertical incision rates. Thus, efforts to identify terraces that record climate signals are best focused on environments where terrace ages and geometries are far different than would be predicted by a constant vertical incision model.

Appendix A

Here we summarize model variables and statistics for terrace age and geometry. Dimensions are indicated in parentheses.

Table A1. Notation

Symbol	Description
	Model Dimensional Variables
w_c	Channel width (L)
h_c	Channel depth (L)
w_{ab}	Initial alluvial belt width (L)
w_{uab}	Initial alluvial belt width, unconfined (L)
C_f	Friction coefficient
E_V	Vertical incision rate (L/T)
E_L	Maximum lateral erosion rate (L/T)
E_{Ls}	Maximum lateral erosion rate in sediment banks (L/T)
E_{Lb}	Maximum lateral erosion rate in bedrock banks (L/T)
k_e	Lateral erosion rate constant (L/T)
k_s	Lateral erosion rate constant, sediment banks (L/T)
k_b	Lateral erosion rate constant, bedrock banks (L/T)
f_b	Fraction of bedrock in bank materials
Δt	Time step (T)
t	Simulation time (T)
$R_o(s)$	Dimensionless lateral erosion rate based on local curvature at centerline node s
$R_1(s)$	Dimensionless lateral erosion rate, incorporating upstream curvature, at centerline node s
$M(s)$	Lateral erosion rate at centerline node s (L/T)
s	Centerline node index
G	Lateral erosion rate weighting function
ξ	Distance along channel (L)
ξ_{max}	Maximum distance along channel for curvature integral (L)
r	Local radius of channel curvature (L)
k	Dimensionless coefficient in weighting function G
ε	Dimensionless exponent for effect of sinuosity on lateral erosion rate
Γ, Ω	Dimensionless lateral erosion rate weighting coefficients
μ	Channel sinuosity
	Model Nondimensional Variables
$t^* = \frac{tE_{Ls}}{w_c}$	Nondimensional simulation time
$E_V^* = \frac{E_V w_c}{E_L h_c}$	Nondimensional vertical incision rate
$E_{Vb}^* = \frac{E_V w_c}{E_{Lb} h_c}$	Nondimensional vertical incision rate with bedrock banks
$E_{Vs}^* = \frac{E_V w_c}{E_{Ls} h_c}$	Nondimensional vertical incision rate with sediment banks
$w_c^* = \frac{w_c}{h_c}$	Channel width-to-depth ratio
$w_{ab}^* = \frac{w_{ab}}{w_{uab}}$	Nondimensional initial alluvial belt width
	Terrace Age Statistics
Δz	Size of elevation bin for distinguishing unique terrace levels (L)
Δz_{50}	Median elevation difference between unique terrace levels (L)
$\Delta t_{terrace}$	Distribution of time intervals between unique terrace levels (i.e., separated vertically by $\Delta z \geq 1$) (T)
$\Delta t_{terrace,90}$	90th percentile of time interval between unique terrace levels (T)
$\Delta t_{terrace,50}$	Median time interval between unique terrace levels (T)
$\Delta t_{terrace,10}$	10th percentile of time interval between unique terrace levels (T)
	Terrace Geometry Statistics
$\varnothing_{terrace}$	Terrace dip direction (degrees), measured counterclockwise from the mean azimuth of the downstream-oriented valley axis
P_{max}	Most probable terrace dip direction
P_{median}	Probability for the median terrace dip direction
$S_{terrace}$	Terrace slope (dimensionless)
$L_{terrace,max}$	Maximum terrace length in the valley-parallel direction (L)
f_{paired}	Fraction of paired terraces (i.e., terraces adjacent, on opposite sides of the channel, and with mean elevation less than 2 m apart) in the model domain, weighted by terrace area

Acknowledgments

This work was supported by the Department of Defense through the National Defense Science and Engineering Graduate Fellowship (NDSEG) Program and NSF grant EAR-1147381 to M.P.L. Acknowledgment is also made to the donors of the American Chemical Society Petroleum Research Fund for partial support of this research. Model data and digitized terrace maps from this manuscript are available upon request. We thank Bob Anderson, Jean-Philippe Avouac, Patrick Belmont, Noah Finnegan, Dirk Scherler, and Andrew Thompson for their insightful discussions. We acknowledge Alexander Densmore, Nicole Gasparini, Alex Whittaker, Stephen Lancaster, and John Buffington for detailed and constructive formal reviews.

References

Amos, C. B., and D. W. Burbank (2007), Channel width response to differential uplift, *J. Geophys. Res.*, *112*, F02010, doi:10.1029/2006JF000672.

Baker, V. R., and M. M. Penteado-Orellana (1977), Adjustment to Quaternary climatic change by the Colorado River in central Texas, *J. Geol.*, *85*(4), 395–422.

Barnes, V. E., et al. (1974a), Austin sheet, 1:250,000 scale, Geologic Atlas of Texas, Bureau of Economic Geology, Austin, Tex.

Barnes, V. E., et al. (1974b), Seguin sheet, 1:250,000 scale, Geologic Atlas of Texas, Bureau of Economic Geology, Austin, Tex.

Ben Moshe, L., I. Haviv, Y. Enzel, E. Zilberman, and A. Matmon (2008), Incision of alluvial channels in response to a continuous base level fall: Field characterization, modeling, and validation along the Dead Sea, *Geomorphology*, *93*(3–4), 524–536, doi:10.1016/j.geomorph.2007.03.014.

Blum, M. D. (1992), Modern depositional environments and recent alluvial history of the lower Colorado River, Gulf Coastal Plain of Texas, PhD thesis, Univ. Texas at Austin, Austin, Tex.

Blum, M. D., and A. Aslan (2006), Signatures of climate vs. sea-level change within incised valley-fill successions: Quaternary examples from the Texas Gulf Coast, *Sediment. Geol.*, *190*(1–4), 177–211, doi:10.1016/j.sedgeo.2006.05.024.

Blum, M. D., and S. Valastro (1994), Late Quaternary sedimentation, lower Colorado River, Gulf Coastal Plain, *Geol. Soc. Am. Bull.*, *106*(8), 1002–1016, doi:10.1130/0016-7606(1994)106<1002:LQSLCR>2.3.CO;2.

Blum, M. D., and T. E. Tornqvist (2000), Fluvial responses to climate and sea-level change: A review and look forward, *Sedimentology*, *47*, 2–48, doi:10.1046/j.1365-3091.2000.00008.x.

Born, S. M., and D. F. Ritter (1970), Modern terrace development near Pyramid Lake, Nevada, and its geologic implications, *Geol. Soc. Am. Bull.*, *81*(4), 1233–1242, doi:10.1130/0016-7606(1970)81[1233:MTDNPL]2.0.CO;2.

Bradley, D. N., and G. E. Tucker (2013), The storage time, age, and erosion hazard of laterally accreted sediment on the floodplain of a simulated meandering river, *J. Geophys. Res. Earth Surf.*, *118*, 1308–1319, doi:10.1002/jgrf.20083.

Brice, J. (1974), Evolution of meander loops, *Geol. Soc. Am. Bull.*, *85*(4), 581–586, doi:10.1130/0016-7606(1974)85<581:EOML>2.0.CO;2.

Bridgland, D., and R. Westaway (2008), Climatically controlled river terrace staircases: A worldwide Quaternary phenomenon, *Geomorphology*, *98*(3–4), 285–315, doi:10.1016/j.geomorph.2006.12.032.

Bucher, W. H. (1932), "Strath" as a geomorphic term, *Science*, *75*(1935), 130–131, doi:10.1126/science.75.1935.130-a.

Bull, W. B. (1990), Stream-terrace genesis: Implications for soil development, *Geomorphology*, *3*, 351–367.

Bull, W. B. (1991), *Geomorphic Responses to Climatic Change*, Oxford Univ. Press, New York.

Burrough, P. A., and R. A. McDonell (1998), *Principles of Geographic Information Systems*, Oxford Univ. Press, New York.

Camporeale, C., P. Perona, A. Porporato, and L. Ridolfi (2005), On the long-term behavior of meandering rivers, *Water Resour. Res.*, *41*, W12403, doi:10.1029/2005WR004109.

Case, J. C., C. S. Arneson, and L. L. Hallberg (1998), Surficial geology map of Wyoming, Wyoming State Geological Survey, Laramie, Wyoming.

Chadwick, O. A., R. D. Hall, and F. M. Phillips (1997), Chronology of Pleistocene glacial advances in the central Rocky Mountains, *Geol. Soc. Am. Bull.*, *109*(11), 1443–1452, doi:10.1130/0016-7606(1997)109<1443:COPGAI>2.3.CO;2.

Challinor, J. (1932), River terraces as normal features of valley development, *Geography*, *17*(2), 141–147.

Davis, W. M. (1909), *Geographical Essays*, Ginn and Co., Boston, Mass.

Demir, T., A. Seyrek, H. Guillou, S. Scaillet, R. Westaway, and D. Bridgland (2009), Preservation by basalt of a staircase of latest Pliocene terraces of the River Murat in eastern Turkey: Evidence for rapid uplift of the eastern Anatolian Plateau, *Global Planet. Change*, *68*(4), 254–269, doi:10.1016/j.gloplacha.2009.02.008.

Demoulin, A., B. Bovy, G. Rixhon, and Y. Cornet (2007), An automated method to extract fluvial terraces from digital elevation models: The Vesdre valley, a case study in eastern Belgium, *Geomorphology*, *91*(1–2), 51–64, doi:10.1016/j.geomorph.2007.01.020.

DeVecchio, D. E., R. V. Heermance, M. Fuchs, and L. A. Owen (2012), Climate-controlled landscape evolution in the western Transverse Ranges, California: Insights from Quaternary geochronology of the Saugus Formation and strath terrace flights, *Lithosphere*, *4*(2), 110–130, doi:10.1130/L176.1.

Dibblee, T. W., and J. A. Minch (2008), *Geologic Map of the Point Delgada and Garberville 15 minute Quadrangles, Humboldt and Mendocino Counties, California*, Dibblee Geological Found., Camarillo, Calif.

DiBiase, R. A., K. X. Whipple, M. P. Lamb, and A. M. Heimsath (2014), The role of waterfalls and knickzones in controlling the style and pace of landscape adjustment in the western San Gabriel Mountains, California, *Geol. Soc. Am. Bull.*, doi:10.1130/B31113.1.

Eke, E. C., G. Parker, and Y. Shimizu (2014), Numerical modeling of erosional and depositional bank processes in migrating river bends with self-formed width: Morphodynamics of bar push and bank pull, *J. Geophys. Res. Earth Surf.*, *119*, 1455–1483, doi:10.1002/2013JF003020.

Erkens, G., R. Dambeck, K. P. Volleberg, M. T. I. J. Bouman, J. A. A. Bos, K. M. Cohen, J. Wallinga, and W. Z. Hoek (2009), Fluvial terrace formation in the northern Upper Rhine Graben during the last 20000 years as a result of allogenic controls and autogenic evolution, *Geomorphology*, *103*(3), 476–495, doi:10.1016/j.geomorph.2008.07.021.

Ferguson, R. I. (1973), Channel pattern and sediment type, *Area*, *5*, 38–41.

Finnegan, N. J. (2013), Interpretation and downstream correlation of bedrock river terrace treads created from propagating knickpoints, *J. Geophys. Res. Earth Surf.*, *118*, 54–64, doi:10.1029/2012JF002534.

Finnegan, N. J., and G. Balco (2013), Sediment supply, base level, braiding, and bedrock river terrace formation: Arroyo Seco, California, USA, *Geol. Soc. Am. Bull.*, *125*(7–8), 1114–1124, doi:10.1130/B30727.1.

Finnegan, N. J., and W. E. Dietrich (2011), Episodic bedrock strath terrace formation due to meander migration and cutoff, *Geology*, *39*(2), 143–146, doi:10.1130/G31716.1.

Finnegan, N. J., G. Roe, D. R. Montgomery, and B. Hallet (2005), Controls on the channel width of rivers: Implications for modeling fluvial incision of bedrock, *Geology*, *33*(3), 229–232, doi:10.1130/G21171.1.

Finnegan, N. J., R. Schumer, and S. Finnegan (2014), A signature of transience in bedrock river incision rates over timescales of 10^4–10^7 years, *Nature*, *505*(7483), 391–394, doi:10.1038/nature12913.

Fisk, H. N. (1944), *Geological Investigation of the Alluvial Valley of the Lower Mississippi River*, Miss. River Comm., Vicksburg, Miss.

Frankel, K. L., F. J. Pazzaglia, and J. D. Vaughn (2007), Knickpoint evolution in a vertically bedded substrate, upstream-dipping terraces, and Atlantic slope bedrock channels, *Geol. Soc. Am. Bull.*, *119*(3–4), 476–486.

Frascati, A., and S. Lanzoni (2010), Long-term river meandering as a part of chaotic dynamics? A contribution from mathematical modelling, *Earth Surf. Processes Landforms*, *35*(7), 791–802, doi:10.1002/esp.1974.

Fuller, T. K., L. A. Perg, J. K. Willenbring, and K. Lepper (2009), Field evidence for climate-driven changes in sediment supply leading to strath terrace formation, *Geology*, *37*(5), 467–470, doi:10.1130/G25487A.1.

Ganti, V., M. P. Lamb, and B. McElroy (2014), Quantitative bounds on morphodynamics and implications for reading the sedimentary record, *Nat. Commun.*, *5*, doi:10.1038/ncomms4298.
Gesch, D. B. (2007), The National Elevation Dataset, in *Digital Elevation Model Technologies and Applications: The DEM Users Manual*, edited by D. Maune, pp. 99–118, American Society for Photogrammetry and Remote Sens., Bethesda, Md.
Gran, K. B., N. Finnegan, A. L. Johnson, P. Belmont, C. Wittkop, and T. Rittenour (2013), Landscape evolution, valley excavation, and terrace development following abrupt postglacial base-level fall, *Geol. Soc. Am. Bull.*, *125*(11/12), 1851–1864, doi:10.1130/B30772.1.
Gran, K., P. Belmont, S. Day, C. Jennings, J. W. Lauer, E. Viparelli, P. Wilcock, and G. Parker (2011), An integrated sediment budget for the Le Sueur River Basin, MPCA Rep. Wq-lw7-29o.
Guneralp, I., and R. A. Marston (2012), Process-form linkages in meander morphodynamics: Bridging theoretical modeling and real world complexity, *Prog. Phys. Geogr.*, *36*(6), 718–746, doi:10.1177/0309133312451989.
Gutierrez, R. R., J. D. Abad, M. Choi, and H. Montoro (2014), Characterization of confluences in free meandering rivers of the Amazon basin, *Geomorphology*, *220*, 1–14, doi:10.1016/j.geomorph.2014.05.011.
Hack, J. T. (1955), Geology of the Brandywine area and origin of the upland of southern Maryland, *U.S. Geol. Surv. Prof. Pap., 267–A,* Washington, D. C.
Hallet, B., L. Hunter, and J. Bogen (1996), Rates of erosion and sediment evacuation by glaciers: A review of field data and their implications, *Global Planet. Change*, *12*(1), 213–235.
Hancock, G. S., and R. S. Anderson (2002), Numerical modeling of fluvial strath-terrace formation in response to oscillating climate, *Geol. Soc. Am. Bull.*, *114*(9), 1131–1142.
Hancock, G. S., R. S. Anderson, O. A. Chadwick, and R. C. Finkel (1999), Dating fluvial terraces with ^{10}Be and ^{26}Al profiles: Application to the Wind River, Wyoming, *Geomorphology*, *27*(1), 41–60.
Hanks, T. C., and R. C. Finkel (2005), Early Pleistocene incision of the San Juan River, Utah, dated with ^{26}Al and ^{10}Be: Comment and reply, *Geology*, *33*(1), e78–e79, doi:10.1130/0091-7613-33.1.e78.
Harden, D. (1990), Controlling factors in the distribution and development of incised meanders in the central Colorado Plateau, *Geol. Soc. Am. Bull.*, *102*(2), 233–242, doi:10.1130/0016-7606(1990)102<0233:CFITDA>2.3.CO;2.
Hays, J. D., J. Imbrie, and N. J. Shackleton (1976), Variations in the Earth's orbit: Pacemaker of the ice ages, *Science*, *194*(4270), 1121–1132.
Hooke, J. M. (2013), 9.16 River Meandering, in *Treatise on Geomorphology*, pp. 260–288, Academic Press, San Diego, Calif.
Howard, A., and A. Hemberger (1991), Multivariate characterization of meandering, *Geomorphology*, *4*(3–4), 161–186, doi:10.1016/0169-555X(91)90002-R.
Howard, A. D. (1996), Modelling channel evolution and floodplain morphology, in *Floodplain Processes*, edited by M. G. Anderson, D. E. Walling, and P. E. Bates, pp. 15–62, John Wiley, Chichester, U. K.
Howard, A. D., and G. Kerby (1983), Channel changes in badlands, *Geol. Soc. Am. Bull.*, *94*(6), 739–752.
Howard, A. D., and T. R. Knutson (1984), Sufficient conditions for river meandering—A simulation approach, *Water Resour. Res.*, *20*(11), 1659–1667, doi:10.1029/WR020i011p01659.
Ikeda, S., G. Parker, and K. Sawai (1981), Bend theory of river meanders: Part 1. Linear development, *J. Fluid Mech.*, *112*(11), 363–377.
Jerolmack, D. J., and C. Paola (2010), Shredding of environmental signals by sediment transport, *Geophys. Res. Lett.*, *37*, L19401, doi:10.1029/2010GL044638.
Lancaster, S. T. (1998), A nonlinear river meandering model and its incorporation in a landscape evolution model, PhD thesis, Massachusetts Institute of Technology, Cambridge, Mass.
Lancaster, S. T., and R. L. Bras (2002), A simple model of river meandering and its comparison to natural channels, *Hydrol. Process.*, *16*(1), 1–26, doi:10.1002/hyp.273.
Langston, A. L., G. E. Tucker, and R. S. Anderson (2015), Interpreting climate-modulated processes of terrace development along the Colorado Front Range using a landscape evolution model, *J. Geophys. Res. Earth Surf.*, *120*, 2121–2138, doi:10.1002/2014JF003403.
Lavé, J., and J. P. Avouac (2000), Active folding of fluvial terraces across the Siwaliks Hills, Himalayas of central Nepal, *J. Geophys. Res.*, *105*(B3), 5735–5770, doi:10.1029/1999JB900292.
Lavé, J., and J. P. Avouac (2001), Fluvial incision and tectonic uplift across the Himalayas of central Nepal, *J. Geophys. Res.*, *106*(B11), 26,561–26,591, doi:10.1029/2001JB000359.
Leopold, L. B., and M. G. Wolman (1960), River meanders, *Geol. Soc. Am. Bull.*, *71*(6), 769–794, doi:10.1130/0016-7606(1960)71[769:RM]2.0.CO;2.
Leopold, L. B., M. G. Wolman, and J. P. Miller (1964), *Fluvial Processes in Geomorphology*, pp. 79–80, Freeman, San Francisco, Calif.
Lewin, J., and B. J. Brindle (1977), Confined meanders, in *River Channel Changes*, edited by K. J. Gregory, pp. 221–233, John Wiley, Chichester, U. K.
Lewin, J., and M. G. Macklin (2003), Preservation potential for late Quaternary river alluvium, *J. Quat. Sci.*, *18*(2), 107–120, doi:10.1002/jqs.738.
Limaye, A. B. S., and M. P. Lamb (2013), A vector-based method for bank-material tracking in coupled models of meandering and landscape evolution, *J. Geophys. Res. Earth Surf.*, *118*, 2421–2437, doi:10.1002/2013JF002854.
Limaye, A. B. S., and M. P. Lamb (2014), Numerical simulations of bedrock valley evolution by meandering rivers with variable bank material, *J. Geophys. Res. Earth Surf.*, *119*, 927–950, doi:10.1002/2013JF002997.
Lusardi, B. A., H. C. Hobbs, and C. J. Patterson (2002), *Surficial Geology of the Faribault 30 × 60 minute Quadrangle, South-Central Minnesota*, Minn. Geological Surv., St. Paul, Minn.
Merritts, D. J., K. R. Vincent, and E. E. Wohl (1994), Long river profiles, tectonism, and eustasy: A guide to interpreting fluvial terraces, *J. Geophys. Res.*, *99*(B7), 14,031–14,050, doi:10.1029/94JB00857.
Mizutani, T. (1998), Laboratory experiment and digital simulation of multiple fill-cut terrace formation, *Geomorphology*, *24*(4), 353–361, doi:10.1016/S0169-555X(98)00027-0.
Molnar, P., E. T. Brown, B. C. Burchfiel, Q. Deng, X. Feng, J. Li, G. M. Raisbeck, J. Shi, W. Zhangming, and F. Yiou (1994), Quaternary climate change and the formation of river terraces across growing anticlines on the north flank of the Tien Shan, China, *J. Geol.*, *102*(5), 583–602.
Montgomery, D. R. (2004), Observations on the role of lithology in strath terrace formation and bedrock channel width, *Am. J. Sci.*, *304*(5), 454–476, doi:10.2475/ajs.304.5.454.
Niviere, B., and G. Marquis (2000), Evolution of terrace risers along the upper Rhine graben inferred from morphologic dating methods: Evidence of climatic and tectonic forcing, *Geophys. J. Int.*, *141*(3), 577–594, doi:10.1046/j.1365-246x.2000.00123.x.
Pan, B., D. Burbank, Y. Wang, G. Wu, J. Li, and Q. Guan (2003), A 900 k.y. record of strath terrace formation during glacial-interglacial transitions in northwest China, *Geology*, *31*(11), 957–960, doi:10.1130/G19685.1.
Parker, G. (1976), On the cause and characteristic scales of meandering and braiding in rivers, *J. Fluid Mech.*, *76*(3), 457–480, doi:10.1017/S0022112076000748.

Parker, G., Y. Shimizu, G. V. Wilkerson, E. C. Eke, J. D. Abad, J. W. Lauer, C. Paola, W. E. Dietrich, and V. R. Voller (2011), A new framework for modeling the migration of meandering rivers, *Earth Surf. Processes Landforms*, *36*(1), 70–86, doi:10.1002/esp.2113.

Pazzaglia, F. J. (2013), Fluvial terraces, in *Treatise on Geomorphology*, vol. 9, edited by E. Wohl, pp. 379–412, Academic Press, San Diego, Calif.

Pazzaglia, F. J., and T. W. Gardner (1993), Fluvial terraces of the lower Susquehanna River, *Geomorphology*, *8*(2), 83–113.

Pazzaglia, F. J., T. W. Gardner, and D. J. Merritts (1998), Bedrock fluvial incision and longitudinal profile development over geologic time scales determined by fluvial terraces, in *Rivers Over Rock: Fluvial Processes in Bedrock Channels*, vol. 107, edited by K. J. Tinkler and E. E. Wohl, pp. 207–235, AGU, Washington, D. C.

Personius, S. (1995), Late Quaternary stream incision and uplift in the forearc of the Cascadia subduction zone, western Oregon, *J. Geophys. Res.*, *100*(B10), 20,193–20,210, doi:10.1029/95JB01684.

Personius, S. F., H. M. Kelsey, and P. C. Grabau (1993), Evidence for regional stream aggradation in the central Oregon Coast Range during the Pleistocene-Holocene transition, *Quat. Res.*, *40*(3), 297–308.

Phillips, J. D., and M. C. Slattery (2006), Sediment storage, sea level, and sediment delivery to the ocean by coastal plain rivers, *Prog. Phys. Geogr.*, *30*(4), 513–530, doi:10.1191/0309133306pp494ra.

Picotti, V., and F. J. Pazzaglia (2008), A new active tectonic model for the construction of the Northern Apennines mountain front near Bologna (Italy), *J. Geophys. Res.*, *113*, B08412, doi:10.1029/2007JB005307.

Rockwell, T. K., E. A. Keller, M. N. Clark, and D. L. Johnson (1984), Chronology and rates of faulting of Ventura River terraces, California, *Geol. Soc. Am. Bull.*, *95*(12), 1466–1474, doi:10.1130/0016-7606(1984)95<1466:CAROFO>2.0.CO;2.

Ryder, J. M., and M. Church (1986), The Lillooet terraces of Fraser River: A palaeoenvironmental enquiry, *Can. J. Earth Sci.*, *23*(6), 869–884, doi:10.1139/e86-089.

Schumm, S. A. (1977), *The Fluvial System*, Wiley, New York.

Seidl, M. A., and W. E. Dietrich (1992), The problem of channel erosion into bedrock, *Catena Suppl.*, *23*, 101–124.

Seminara, G. (2006), Meanders, *J. Fluid Mech.*, *554*(1), 271–297, doi:10.1017/S0022112006008925.

Sklar, L. S., and W. E. Dietrich (2001), Sediment and rock strength controls on river incision into bedrock, *Geology*, *29*(12), 1087–1090, doi:10.1130/0091-7613(2001)029<1087:SARSCO>2.0.CO;2.

Smalley, M. L., W. W. Emmett, and A. M. Wacker (1994), Annual replenishment of bed material by sediment transport in the Wind River near Riverton, Wyoming, *U.S. Geol. Surv. Water Res. Invest. Rep., 94-4007*.

Stark, C. P. (2006), A self-regulating model of bedrock river channel geometry, *Geophys. Res. Lett.*, *33*, L04402, doi:10.1029/2005GL023193.

Stark, C. P., J. R. Barbour, Y. S. Hayakawa, T. Hattanji, N. Hovius, H. Chen, C.-W. Lin, M.-J. Horng, K.-Q. Xu, and Y. Fukahata (2010), The climatic signature of incised river meanders, *Science*, *327*(5972), 1497–1501, doi:10.1126/science.1184406.

Stølum, H.-H. (1996), River meandering as a self-organization process, *Science*, *271*(5256), 1710–1713, doi:10.1126/science.271.5256.1710.

Stout, J. C., and P. Belmont (2013), TerEx Toolbox for semi-automated selection of fluvial terrace and floodplain features from lidar, *Earth Surf. Processes Landforms*, *39*(5), 569–580, doi:10.1002/esp.3464.

Stricklin, F. L. (1961), Degradational stream deposits of the Brazos River, central Texas, *Geol. Soc. Am. Bull.*, *72*(1), 19–36.

Sun, T., P. Meakin, T. Jossang, and K. Schwarz (1996), A simulation model for meandering rivers, *Water Resour. Res.*, *32*(9), 2937–2954, doi:10.1029/96WR00998.

Tinkler, J., and E. Wohl (1998), *Rivers Over Rock: Fluvial Processes in Bedrock Channels*, *Geophys. Monogr. Ser.*, AGU, Washington, D. C.

Turowski, J. M., N. Hovius, H. Meng-Long, D. Lague, and C. Men-Chiang (2008), Distribution of erosion across bedrock channels, *Earth Surf. Processes Landforms*, *33*(3), 353–363, doi:10.1002/esp.1559.

Tyráček, J., R. Westaway, and D. Bridgland (2004), River terraces of the Vltava and Labe (Elbe) system, Czech Republic, and their implications for the uplift history of the Bohemian Massif, *Proc. Geol. Assoc.*, *115*(2), 101–124, doi:10.1016/S0016-7878(04)80022-1.

van den Berg, M. W. (1996), Fluvial sequences of the Maas: A 10 Ma record of neotectonics and climatic change at various time-scales, PhD thesis, Wageningen Agricultural Univ., Netherlands.

van den Berg, M. W., and T. van Hoof (2001), The Maas terrace sequence at Maastricht, SE Netherlands: Evidence for 200 m of late Neogene and Quaternary surface uplift, in *River Basin Sediment Systems: Archives of Environmental Change*, pp. 45–86, Abingdon, U. K.

Veldkamp, A., and J. J. van Dijke (2000), Simulating internal and external controls on fluvial terrace stratigraphy: A qualitative comparison with the Maas record, *Geomorphology*, *33*(3–4), 225–236, doi:10.1016/S0169-555X(99)00125-7.

Wegmann, K. W., and F. J. Pazzaglia (2002), Holocene strath terraces, climate change, and active tectonics: The Clearwater River basin, Olympic Peninsula, Washington State, *Geol. Soc. Am. Bull.*, *114*(6), 731–744.

Wegmann, K. W., and F. J. Pazzaglia (2009), Late Quaternary fluvial terraces of the Romagna and Marche Apennines, Italy: Climatic, lithologic, and tectonic controls on terrace genesis in an active orogen, *Quat. Sci. Rev.*, *28*(1–2), 137–165, doi:10.1016/j.quascirev.2008.10.006.

Weldon, R. J. (1986), The late Cenozoic geology of Cajon Pass: Implications for tectonics and sedimentation along the San Andreas Fault, PhD thesis, California Institute of Technology, Pasadena, Calif.

Whipple, K. X. (2004), Bedrock rivers and the geomorphology of active orogens, *Annu. Rev. Earth Planet. Sci.*, *32*(1), 151–185, doi:10.1146/annurev.earth.32.101802.120356.

Williams, G. P. (1986), River meanders and channel size, *J. Hydrol.*, *88*(1–2), 147–164, doi:10.1016/0022-1694(86)90202-7.

Wolkowinsky, A. J., and D. E. Granger (2004), Early Pleistocene incision of the San Juan River, Utah, dated with ^{26}Al and ^{10}Be, *Geology*, *32*(9), 749–752, doi:10.1130/G20541.1.

Yanites, B. J., and G. E. Tucker (2010), Controls and limits on bedrock channel geometry, *J. Geophys. Res.*, *115*, F04019, doi:10.1029/2009JF001601.

Yanites, B. J., G. E. Tucker, K. J. Mueller, and Y.-G. Chen (2010), How rivers react to large earthquakes: Evidence from central Taiwan, *Geology*, *38*(7), 639–642, doi:10.1130/G30883.1.